Histone H3 clipping is a novel signature of human neutrophil extracellular traps

Authors

Dorothea O Tilley[1], Ulrike Abuabed[2], Ursula Zimny Arndt[3], Monika Schmid[3], Stefan Florian[4], Peter R. Jungblut[3], Volker Brinkmann[2], Alf Herzig*[1], Arturo Zychlinsky*[1]

Author affiliations

[1]Department of Cellular Microbiology, Core facilities for [2]Microscopy and [3]Protein Analysis, Max Planck Institute for Infection Biology, Charitéplatz 1, 10117 Berlin.

[4]Institut für Pathologie Charité - Universitätsmedizin Berlin, Charitéplatz 1, 10117 Berlin.

*shared last authorship

Abstract

Neutrophils are critical to host defence, executing diverse strategies to perform their antimicrobial and regulatory functions. One tactic is the production of neutrophil extracellular traps (NETs). In response to certain stimuli neutrophils decondense their lobulated nucleus and release chromatin into the extracellular space through a process called NETosis. However, NETosis, and the subsequent degradation of NETs, can become dysregulated. NETs are proposed to play a role in infectious as well as many non-infection related diseases including cancer, thrombosis, autoimmunity and neurological disease. Consequently, there is a need to develop specific tools for the study of these structures in disease contexts. In this study, we identified a NET-specific histone H3 cleavage event and harnessed this to develop a cleavage site-specific antibody for the detection of human NETs. By microscopy, this antibody distinguishes NETs from chromatin in purified and

mixed cell samples. It also detects NETs in tissue sections. We propose this antibody as a new tool to detect and quantify NETs.

Introduction

Neutrophil extracellular traps (NETs) are extracellular structures consisting of chromatin components, including DNA and histones, and neutrophil proteins (Brinkmann et al., 2004, Urban et al., 2009). NETs were first described as an antimicrobial response to infection, facilitating trapping and killing of microbes (Brinkmann et al., 2004). They are found in diverse human tissues and secretions where inflammation is evident (recently reviewed by Sollberger et al., 2018). NETs are produced in response to a wide-range of stimuli; bacteria (Brinkmann et al., 2004); fungi (Urban et al., 2006); viruses (Saitoh et al., 2012; Schonrich et al., 2015); crystals (Schauer et al., 2014); and mitogens (Amulic et al., 2017). Both NADPH oxidase (NOX) dependent and NOX independent mechanisms lead to NET formation (Bianchi et al., 2009; Hakkim et al., 2011; Kenny et al., 2017; Neeli and Radic, 2013). NETs are also observed in sterile disease, including multiple types of thrombotic disease (recently reviewed by Jimenez-Alcazar et al., 2017) and even neurological disease (Zenaro et al., 2015). NETs, or their components, are implicated in the development and exacerbation of autoimmune diseases including psoriasis, vasculitis and systemic lupus erythematosus (recently reviewed by Papayannopoulos, 2018) as well as cancer and cancer metastasis (Albrengues et al., 2018; Cools-Lartigue et al., 2013; Demers et al., 2016). Consequently, there is an urgency across multiple fields to establish the pathological contribution of NETs to disease. However, the detection of NETs in affected tissues remains a challenge.

NETs are histologically defined as areas of decondensed DNA and histones that colocalise with neutrophil granular or cytoplasmic proteins. Thus, reliable detection of NETs requires a combination of anti-neutrophil and anti-chromatin antibodies as well as DNA stains. Immunofluorescent microscopy is a useful method to detect NETs in tissue sections and *in vitro* experiments. However, this can be challenging since NET components are distributed across the large decondensed

48 structure resulting in a weak signal. For example, the signal of antibodies to neutrophil elastase
49 (NE) is significantly dimmer in NETs than in the granules of resting cells where this protease is
50 highly concentrated. Conversely, anti-histone antibodies stain NETs strongly but not nuclei of naïve
51 neutrophils, where the chromatin is compact and less accessible. This differential histone staining
52 property can be exploited for the detection and quantification of NETs (Brinkmann et al., 2012).
53 However, sample preparation and the subsequent image analysis make results between different
54 labs difficult to compare. Thus, there is a need to identify antibodies against NET antigens.

55 NETs can also be detected through post-translational modifications (PTMs) that occur during
56 NETosis. Histone 3 (H3) is deaminated in arginine residues - the conversion to citrulline
57 (citrullination) - by protein arginine deiminase 4 (PAD4) (Wang et al., 2009). Citrullinated H3 (H3cit)
58 is widely used as a surrogate marker of NETs in both *in vitro* and *in vivo* experiments (Gavillet et
59 al., 2015; Pertiwi et al., 2018; Wang et al., 2009; Yoo et al., 2014; Yoshida et al., 2013). Cleavage
60 of histones by granular derived neutrophil serine proteases (NSPs) also contributes to NETosis
61 (Papayannopoulos et al., 2010). Histone cleavage, or clipping, by cysteine or serine proteases is a
62 bona fide histone PTM that facilitates the gross removal of multiple, subtler, PTMs in the histone
63 tail and is conserved from yeast to mammals (Dhaenens et al., 2015). Until now, histone clipping
64 has not been exploited for the detection of NETs but recent work by our group showed that histone
65 H3 cleavage is a conserved response to diverse NET stimuli, including *Candida albicans* and Group
66 B Streptococcus (Kenny 2017). Thus, in this study we map the site(s) of histone H3 cleavage during
67 NETosis. We developed a new monoclonal antibody against cleaved H3 that detects human NETs
68 *in vitro* and in histological samples. This antibody also facilitates easier NET quantification.

Results

Serine protease dependent cleavage of Histone H3 N-terminal tails during NET formation

Histones are processed in response to phorbol 12 myristate 13 acetate - PMA (Papayannopoulos et al., 2010; Urban et al., 2009) and other NET stimuli (Kenny et al., 2017). Indeed, the cleavage products of H3 were consistent between stimuli (Kenny et al., 2017). This suggests that H3 proteolysis occurs at specific sites during NETosis. In a time course experiment of human neutrophils incubated with PMA, we detected a H3 cleavage product of ~14 kDa as early as 30 min post-stimulation (Fig.1A). Further cleavages occurred between 60 and 90 min, yielding products of approximately 13 kDa and 10 kDa, respectively. The histone N-terminal tails protrude from the nucleosome core and are a major PTM target (Bannister and Kouzarides, 2011). A C-terminal, but not an N-terminal, histone antibody detected the cleavage products of H3 (Fig. 1A). These results indicate that the N-terminus is cleaved in truncated H3.

Neutrophil azurophilic granules are rich in serine proteases that can degrade histones *in vitro* (Papayannopoulos et al., 2010). We tested the contribution of these proteases to H3 cleavage during NET formation. Preincubation with the serine protease inhibitor, AEBSF (4- [2-aminoethyl] benzensulfonylfluoride) (Fig. 1A), but not with the cysteine protease inhibitor E64 (S.Fig 1A), inhibited H3 cleavage upon PMA stimulation. AEBSF also inhibited NET formation and nuclear decondensation as shown by immunofluorescent microscopy (Fig. 1B). PMA induced NETosis requires NADPH oxidase activity and, at high concentrations, AEBSF can inhibit activation of NAPDH oxidase (Diatchuk et al., 1997). To rule out this upstream effect, we showed that AEBSF did not inhibit ROS production at the concentrations used in our assay (S.Fig 1B [i]). Similarly, we verified that at these concentrations AEBSF was not cytotoxic, as shown by limited LDH release (S.Fig 1B [ii]). This data shows that serine proteases cleave the N-terminus of H3 early during NET formation.

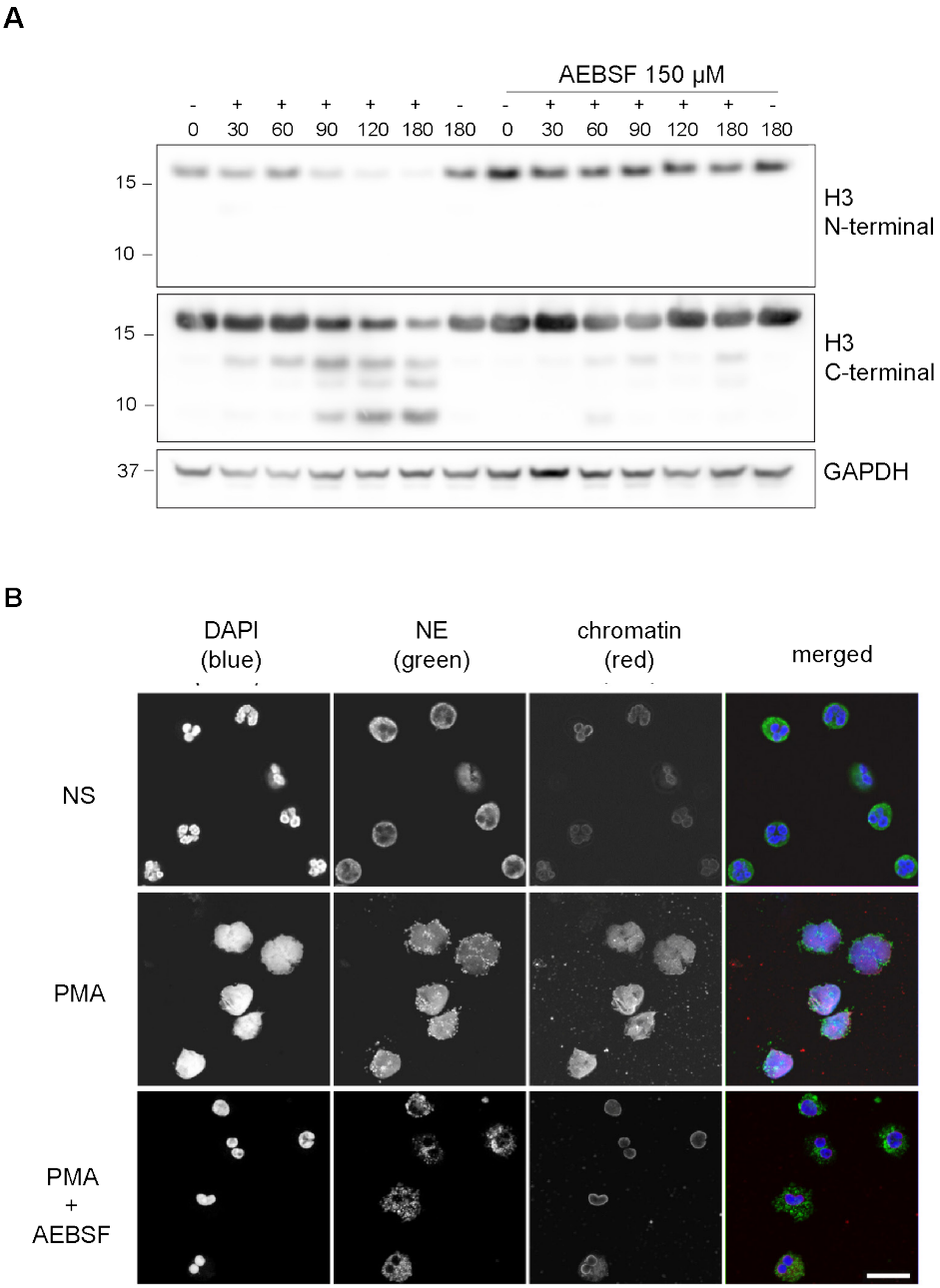

Fig 1. PMA induced Histone H3 cleavage occurs in the N-terminal domain & is prevented by serine protease inhibition.

(**A**) Neutrophils were preincubated with the serine protease inhibitor AEBSF for 30 min in microcentrifuge tubes and then stimulated with PMA as indicated in the figure. Lysates were resolved by SDS-PAGE and immunoblotted with N- and C-terminal antibodies to H3. GAPDH was used as a loading control. (**B**) Immunofluorescent confocal microscopy of NET formation. Neutrophils were seeded on coverslips and preincubated with AEBSF before stimulation with PMA (50 nM) as indicated in the figure. At 150 min the cells were fixed and stained for neutrophil elastase (NE), chromatin (using a H2A-H2B-DNA antibody PL2.3) and DNA (DAPI [4′,6-diamidino-2-phenylindole]). NS: non-stimulated. Images were taken at 63X and the scale bar is 20 μm. Blots and images are representative of 3 independent experiments.

104 *Histone H3 is cleaved at a novel site in the globular domain*

105 To identify the precise H3 cleavage sites we prepared histone enriched extracts from primary
106 neutrophils stimulated with PMA for 90 min and then purified H3 by RP-HPLC as previously
107 described (Shechter et al., 2007). A schematic summary of this is presented in S.Fig. 2A. We
108 identified the fractions containing H3 and its cleaved products by Western blot with anti-H3 C-
109 terminal antibodies (Fig.2A). As expected, H3 was the last core histone to elute (at 45-46 min).

110 We further separated H3 and its truncated forms by two-dimensional electrophoresis (2-DE) and
111 confirmed their identity by mass spectrometry (Fig. 2B and S.Fig. 2B i-ii). The sequence coverage
112 did not include residues that allowed the differentiation of H3 variants. The N-terminals of the
113 separated H3 fragments were not covered by MS and therefore sequenced by Edman degradation
114 from 2 independent experiments (Fig. 2C). The N-terminal sequence of the largest molecular
115 weight H3 spot matched that of intact H3 (Fig 2B, spot 1). We did not obtain reliable sequencing of
116 spots 2 and 3 but the cleavage sites of spots 4 and 5 were identified. The most truncated H3
117 fragment (spot 5) was cleaved between L48 and R49, in the globular domain of the protein, within
118 the nucleosome core structure (Fig. 2D). This is a previously unidentified cleavage site in H3 and,
119 thus, we selected cleavage at H3R49 as a candidate marker of NETs.

120

121

122

123
124
125
126
127

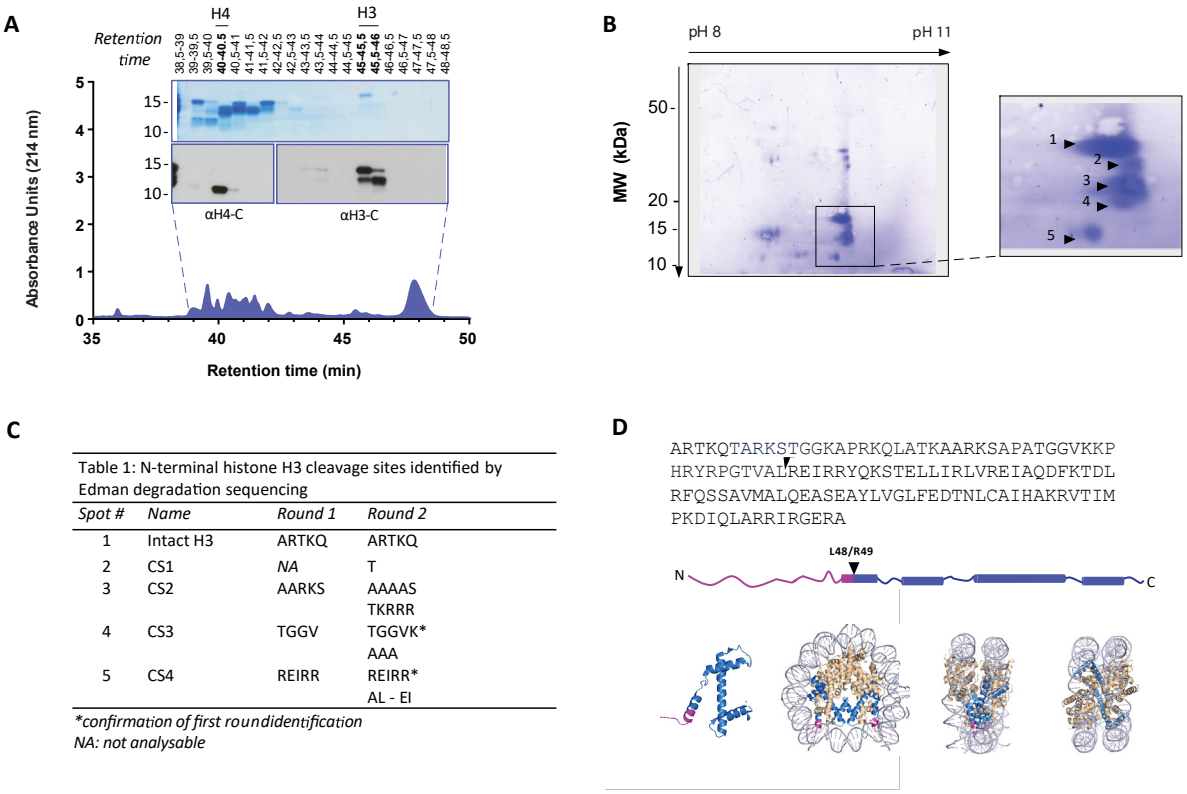

Table 1: N-terminal histone H3 cleavage sites identified by Edman degradation sequencing

Spot #	*Name*	*Round 1*	*Round 2*
1	Intact H3	ARTKQ	ARTKQ
2	CS1	*NA*	T
3	CS2	AARKS	AAAAS TKRRR
4	CS3	TGGV	TGGVK* AAA
5	CS4	REIRR	REIRR* AL - EI

**confirmation of first roundidentification*
NA: not analysable

Fig 2. Identification of histone H3 cleavage sites in NET formation.
(**A**) Representative RP-HPLC chromatogram of acid extracted histones from NETs and corresponding 1D-SDS-PAGE and immunoblots to identify H3 and H4 containing fractions. Histone enriched supernatants were prepared from neutrophils stimulated with PMA for 90 min. (**B**) Representative Coomassie stained blot of pooled H3 fractions separated by 2-DE. Inset is a zoom of all spots (1-5) identified as histone H3 by mass spectrometry. Other proteins identified are listed in the supplementary figures. (**C**) Summary of Edman degradation sequencing results of the H3 spots in two independent experiments. In the second experiment overlapping sequences were detected. However, the detected amino acids for spot 4 and 5 confirmed the initial sequence identification from round 1*. (**D**) Schematic representation of the cleavage site of the truncated H3 product in both the linear sequence of H3 and in the nucleosomal context. H3 is represented in blue and the pink tail region and partial alpha helix represent the part of H3 that is removed. The nucleosome structure is adapted from PDB 2F8N (Chakravarthy, 2005).

Generation of a histone H3 cleavage site monoclonal antibody

We adopted a similar strategy to Duncan and colleagues (2008) to raise antibodies against the cleaved site. We designed a lysine branched immunogen containing the 5 amino acids at the carboxylic side of the H3R49 cleavage site (outlined in S.Fig 3A) and used it to immunize mice. After preliminary screening by ELISA against the immunogen and control peptides, we selected sera, and later hybridoma clones, that detected cleaved H3 in immunoblots of PMA stimulated cell

171 lysates. We excluded sera and clones that detected full length histone H3 in addition to cleaved H3
172 (Fig 3A). We selected sera and clones that detected NETs but not resting chromatin of naive
173 neutrophils by immunofluorescence microscopy. Of the 6 mice immunised, we obtained one stable
174 clone, 3D9, that functioned in both Western blot and microscopy – other clones performed only in
175 Western blot (data not shown). 3D9 recognised a protein of ~10 kDa in neutrophils stimulated with
176 PMA for 120 min and longer but did not detect any protein in resting or early stimulated cells (Fig
177 3A). This band corresponded in size with the smallest H3 fragment detected by the H3 C-terminal
178 antibody. Interestingly, by microscopy, 3D9 exclusively recognised neutrophils undergoing
179 NETosis – with decondensing chromatin (Fig 3B). To validate the specificity of the antibody for the
180 *de novo* N-terminal H3 epitope of NETs, we performed competition experiments with the
181 immunising peptide and demonstrated that it could block 3D9 binding to NETs as shown by
182 immunofluorescent microscopy (S.Fig 3B).

183 3D9 binds specifically to cleaved H3. This antibody binds to the immunizing peptide and to isolated
184 NETs, but not to equal concentrations of chromatin, recombinant H3 or purified calf thymus DNA,
185 by direct ELISA (Fig 3C). Furthermore, in immunoprecipitation experiments, 3D9, but not an isotype
186 control, pulled down intact H3 in lysates of naïve and activated neutrophils, but only the cleaved
187 fragment from activated cells (S.Fig 3C). We detected these pull downs both by Coomassie and
188 silver stained gels. In a similar experiment, we immunoblotted the immunoprecipitate with the C-
189 terminal antibody as well as 3D9 (S.Fig 3C [ii]), and showed that only our monoclonal antibody
190 recognizes cleaved H3. Together this data shows that 3D9 is selective for cleaved H3 under the
191 denaturing conditions of SDS-PAGE but also recognizes full length H3 under the more native
192 conditions of IP.

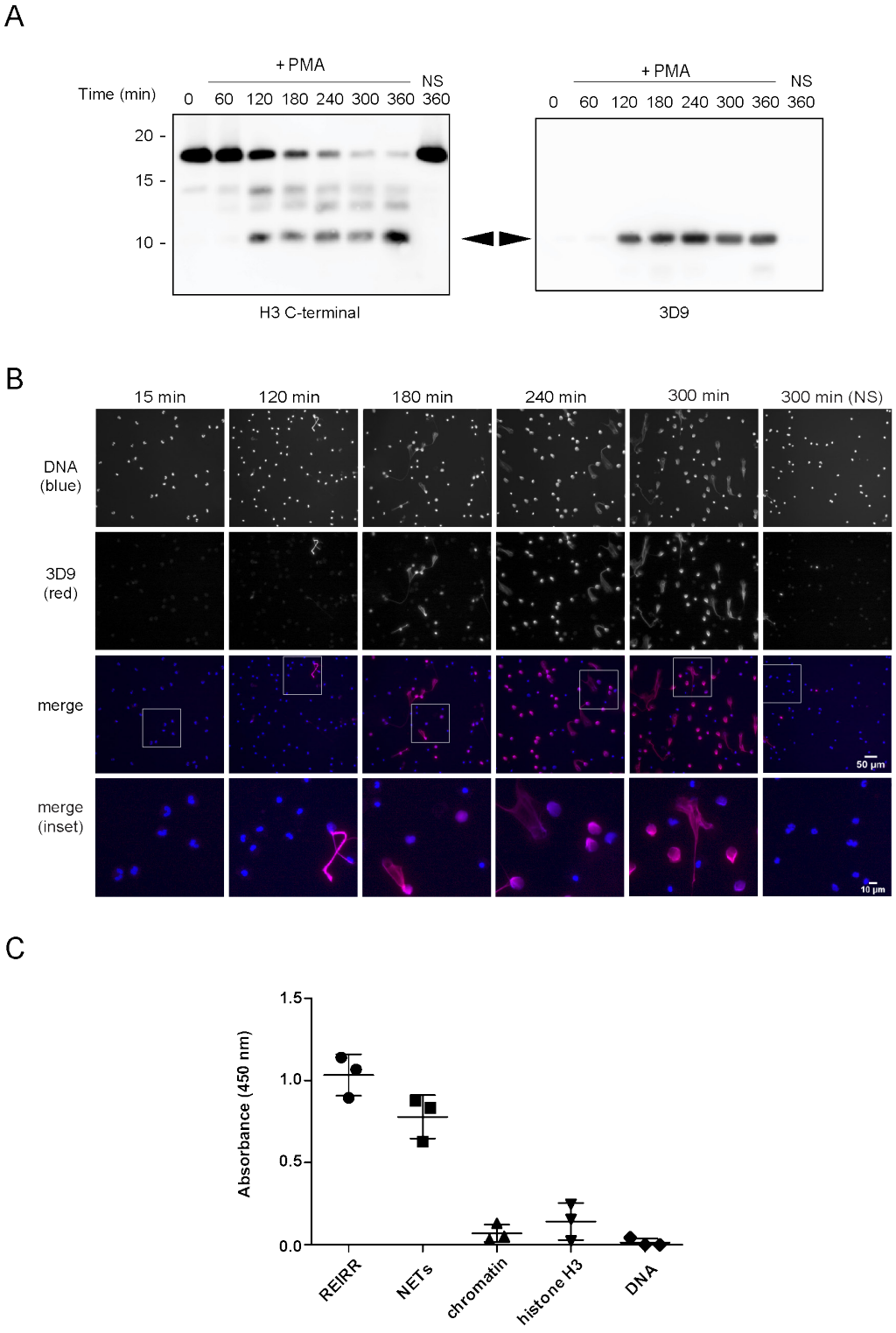

Fig 3. Screening and detection of cleaved H3 & NETs by 3D9
(**A**) Immunoblots of lysates prepared from neutrophils stimulated with PMA (50 nM) for the times indicated in the figure. H3 C-terminal antibody was used as a control to detect all H3 forms while a single band (cleaved H3) was detected by the newly generated monoclonal antibody, 3D9. (**B**) Immunofluorescent microscopy of neutrophils stimulated with PMA and fixed at the indicated times. Samples were stained with Hoechst (DNA - blue) and 3D9 (with Alexafluor-568 conjugated secondary antibody - red). NS: non-stimulated. Images were

taken on an upright fluorescent microscope at 20X. Scale bars – 50 µm (full field) and 10 µm (inset) (**C**) Direct ELISA for cleaved H3 in NETs, chromatin (A549 lung epithelial cells), recombinant histone H3 and DNA. Samples were serially diluted and immobilized on a high affinity ELISA plate according to DNA content (for NETs, chromatin and DNA) or protein content (for recombinant histone H3) as determined by PicoGreen and bicinchoninic acid assays respectively. Starting concentration was 1 µg/ml DNA or protein. Cleaved H3 was detected using 3D9 (2 µg/ml) and HRP conjugated anti-mouse secondary antibody and reactions were developed using TMB (3,3',5,5'-tetramethylbenzidine) as a substrate. Data is presented for dilution 200 ng/ml. REIRR peptide control was coated at 20 ng/ml. Data represents mean ± SD of 3 experiments using independent NET donors.

Epitope mapping

To determine the binding site of 3D9 in histone H3, we tested the antibody by ELISA with overlapping linear peptide arrays and helical peptide mimic arrays (S.file 1) based on a sequence (residues 30-70; PATGGVKKPHRYRPGTVALREIRRYQKSTELLIRKLPFQRL) around the H3R49 cleavage site (S.Fig 4A & 4B). In such assays acetylation is often used to neutralise the contribution of the amino terminal charge. However, to mimic any potential charge created at the newly revealed N-terminus, R49, we also included arrays of unmodified peptides. Based on overlapping peptides, the putative core epitope in the linear array was (R)EIRR. The peptides ending in REIRR were in all cases in the top 2 of each peptide mimic (S.Table 3). Interestingly, peptides extended at the N-terminus were still recognized. Moreover, acetylation at the N-terminus of the peptide ending in the REIRR sequence did not affect the binding, suggesting that a free N-terminus may not be recognized by the antibody. We further refined the epitope mapping by amino acid replacement analysis of linear peptides and helical peptide mimetics ending in REIRR (S.Fig 4C [i, ii]). Mutations in Glu51, Ile52, and Arg54 negatively impacted the signal, indicating these residues are critical for epitope recognition. A schematic of the antibody epitope mapped onto H3 is presented in S.Fig 4C (iii).

Automatic quantification of in vitro generated NETs by microscopy

We tested how 3D9 stained NETs in immunofluorescence in samples that were robustly permeabilized (Triton X-100, 0.5% for 10 min) to facilitate the distribution of the antibody throughout the sample. Fig 4A shows that 3D9 detects decondensed chromatin almost exclusively. In contrast, the anti-chromatin antibody (PL2.3) - directed against a H2A-H2B-DNA epitope (Losman et al.,

231 1992) – stains NETs in addition to condensed nuclei. We compared the staining characteristics of
232 3D9 and PL2.3 during NET formation. We determined the nuclear area and signal intensity at the
233 indicated time points, from multiple fields of view (Fig. 4B). Both antibodies detect the increase in
234 nuclear area characteristic of NETosis between 15 and 180 min after simulation. At later time
235 points, the intensity of PL2.3 staining decreased and failed to discriminate between resting cell
236 nuclei and NETs. In contrast, 3D9 stained nuclei undergoing NETosis more brightly than nuclei of
237 non-activated cells.

238 Publicly available software (ImageJ) can be used to quantify *in vitro* NETosis. We compared 3D9
239 versus the anti-chromatin antibody with our previously published semi-automatic image analysis
240 (Brinkmann et al., 2012) and with a modified automatic method (S.Fig 5A). Both methods use
241 automatic thresholding of the DNA channel (Hoechst) to count total cells/objects. The historical
242 semi-automatic method exploits the differential staining by chromatin antibodies of decondensed
243 chromatin (high signal) over compact chromatin (weak signal) to count cells in NETosis. This
244 method uses a manual thresholding and segmentation procedure (denoted manual in the figure).
245 This manual thresholding step is subject to observer bias. In contrast, the modified method uses
246 automatic thresholding at both stages; total cell and NET counts. Both methods use a size
247 exclusion particle analysis step so that only structures larger than a resting nucleus are counted.
248 Both 3D9 and PL2.3 antibodies effectively quantified NETs using previously published method (Fig
249 4C - manual). However, PL2.3 failed to accurately quantify the number of NETs with the fully
250 automatic method, specifically at early time points after stimulation (15 min). In this case, the weakly
251 staining lobulated nucleus can extend over a larger surface area during cell activation and adhesion
252 resulting in these cells being wrongly categorised as NETs by the algorithm. Together, these data
253 indicate that the automatic method using 3D9 staining can reduce experimental bias.

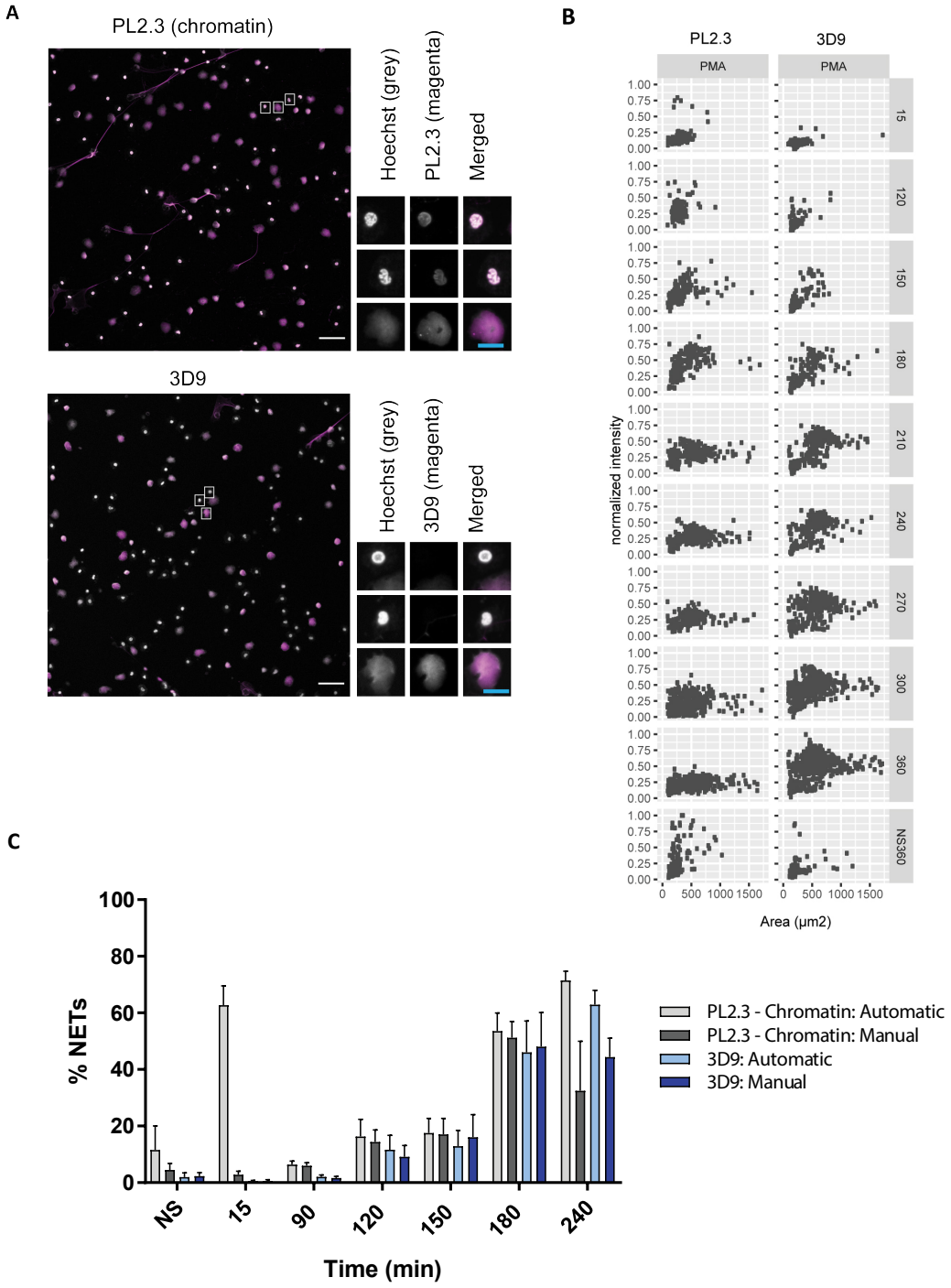

Fig 4. Comparison of NET quantification using an anti-chromatin antibody versus 3D9
(**A**) Confocal immunofluorescent microscopy of neutrophils stimulated with PMA (180 min) and stained with Hoechst and anti-chromatin antibody (PL2.3) or 3D9. Insets represent selected cells examined at higher magnification (63X) and presented as split channels in grayscale or merged as per the total field of view (20X magnification). White scale bar - 50 µm, cyan scale bar - 10 µm. Images are representative of 3 experiments (**B**) Comparison of the fluorescent distribution of PL2.3 versus 3D9 staining of PMA stimulated cells over time (6h). Staining intensities were normalized over all images of the respective time course. NS:360: non-stimulated at 360 min. Analysis is performed on one data set that is representative of 3-4 independent time course experiments. (**C**) Comparison of NET quantification using manual or automatic thresholding and segmentation procedures for chromatin antibody (PL2.3) and cleaved H3 antibody (or 3D9). Manual

thresholding excludes cells/NETs with a weak signal whereas automatic thresholding includes all objects irrespective of signal. Images for analysis were taken using a fluorescence microscope. Graph represents the mean ± standard deviation, where n=3-4.

3D9 detects NETs induced by multiple stimuli

Histone H3 cleavage is a feature of the neutrophil response to multiple NET stimuli (Kenny et al., 2017). 3D9 detects NETs induced by the bacterial toxin nigericin, which induces NETs independently of NADPH oxidase activation (Kenny et al., 2017), by heme in TNF primed neutrophils (Knackstedt et al., 2019) and by the fungal pathogen *Candida albicans* (Fig 5). Interestingly, in *C. albicans* infections, we detected both 3D9 positive and negative NETs.

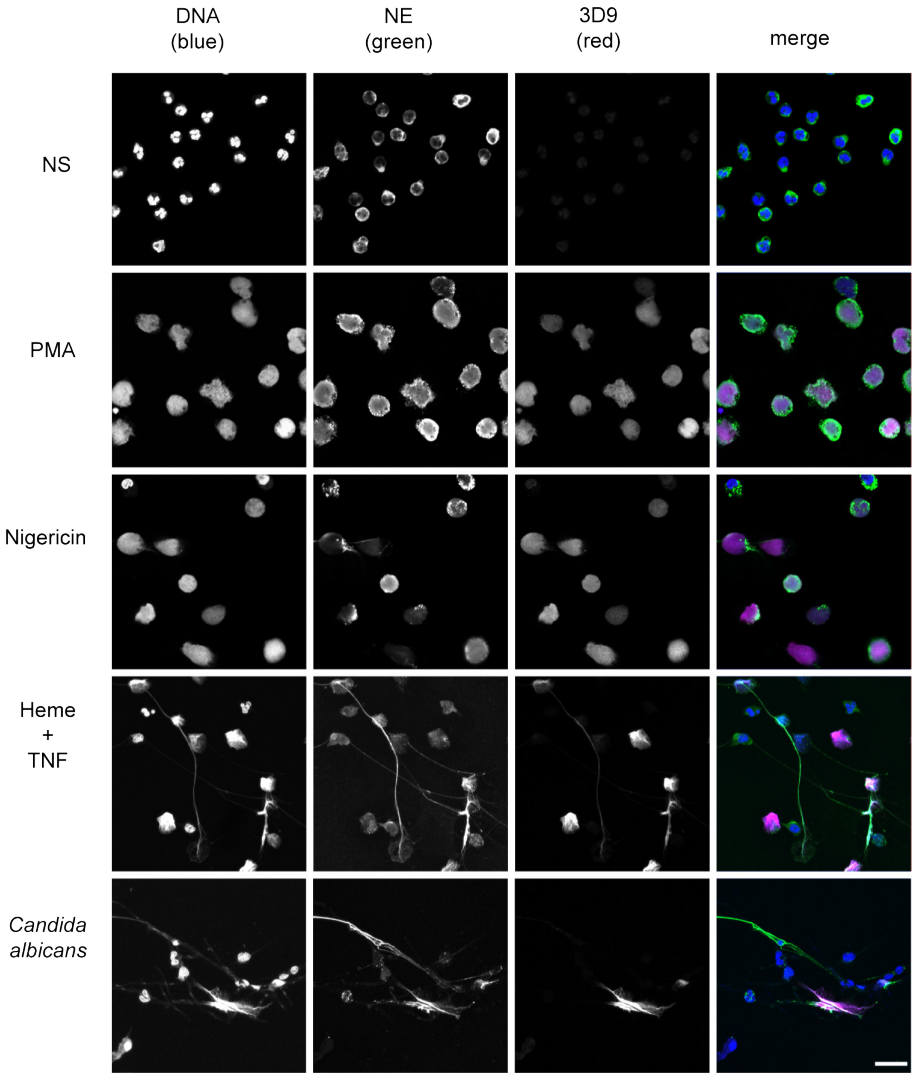

279 **Fig 5. Detection by 3D9 of NETs from diverse stimuli.**
280 Immunofluorescence microscopy of neutrophils left unstimulated (NS), stimulated with PMA (50 nM, 2.5h),
281 nigericin (15 μM, 2.5 h), TNF primed and then stimulated with heme (20 μM, 6h), and neutrophils co-cultured
282 with *Candida albicans* hyphae (MOI 5) for 4h. Samples were stained with Hoechst, anti-neutrophil elastase
283 (NE) and 3D9. Scale bar – 50 μm. Images were taken on a confocal microscope at 20X and are
284 representative of 3 experiments with independent donors. Scale bar - 20 μm.
285

286 *3D9 distinguishes NETs in mixed cell samples*

287 Histone H3 clipping, albeit at other sites in the N-terminal tail, was observed in mast cells (Melo et
288 al., 2014) and unstimulated PBMC fractions (Howe and Gamble, 2015). Of note, PBMC fractions
289 often contain contaminating neutrophils (Hacbarth and Kajdacsy-Balla, 1986). To test if 3D9
290 specifically stained neutrophils treated with NET stimuli, we incubated PBMCs with PMA or
291 nigericin (Fig. 6). Importantly, 3D9 detected only nuclei that appeared decondensed in cells that
292 were positive for NE, a specific neutrophil marker. In contrast, the chromatin antibody stained both
293 neutrophils in NETosis and nuclei of other cells. This shows that 3D9 detects NETs specifically
294 even in the presence of other blood cells.

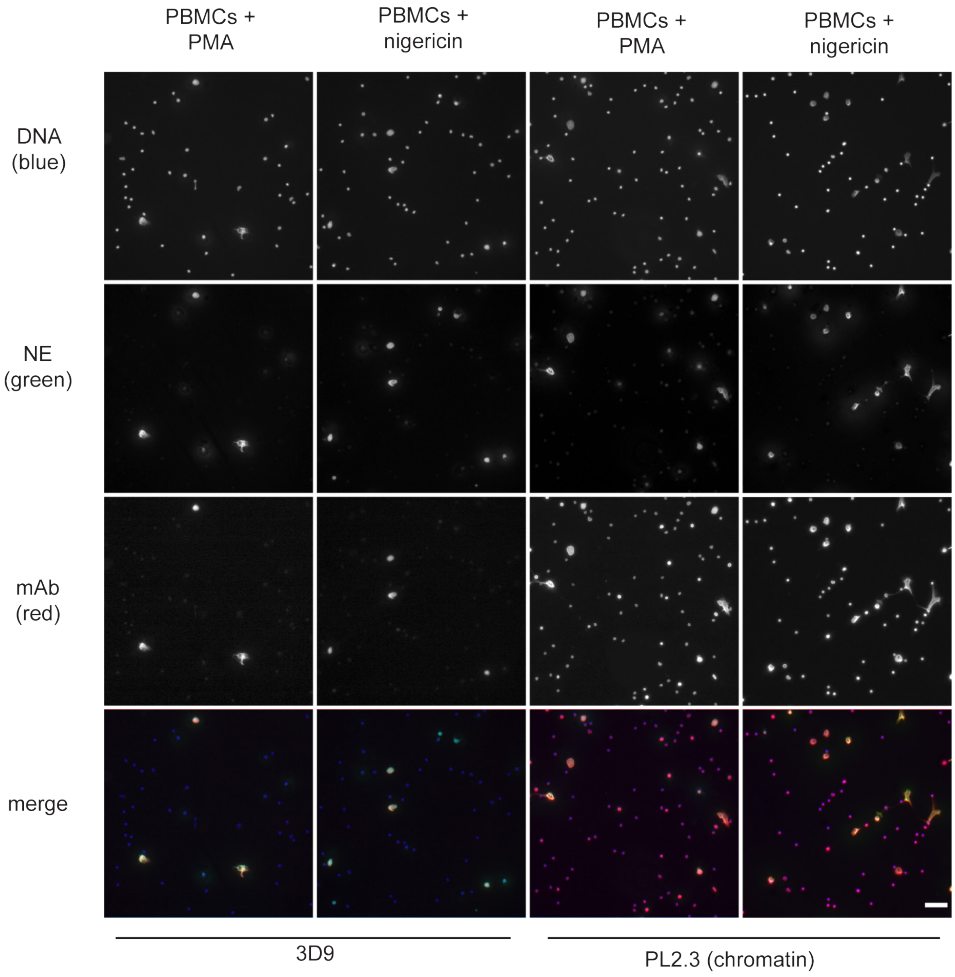

295

296 **Fig 6. Detection of NETs in mixed cell fractions**
297 Immunofluorescence microscopy of non-purified peripheral blood mononuclear cell (PBMC) fractions treated
298 with the NET stimuli, PMA (50 nM, 2.5h) or nigericin (15 μM, 2.5 h), and then stained with Hoechst, anti-
299 neutrophil elastase (NE) and 3D9 or PL2.3. Images were taken on an upright fluorescent microscope at 20X
300 magnification. The selected images are representative of 3 independent experiments. Scale bar – 50 μm.
301
302

303 *3D9 distinguishes NETosis from other forms of cell death in neutrophils*

304 Neutrophils can commit to other cell death pathways (recently reviewed by Dabrowska et al., 2019)
305 besides NETosis. Naïve neutrophils undergo apoptosis after overnight incubation (Kobayashi et
306 al., 2005) and necroptosis upon TNFα stimulation in the presence of a SMAC (second
307 mitochondria-derived activator of caspase) mimetic and if caspases are inhibited (Galluzzi et al.,
308 2012). Interestingly, the anti-chromatin antibody (S.Fig7), but not 3D9, stained the condensed
309 nuclei of cells undergoing apoptosis (Fig. 7) and neither of the antibodies stained cells during

310 necrosis induced by the staphylococcal toxin α-haemolysin nor after stimulation with necroptosis

311 inducers.

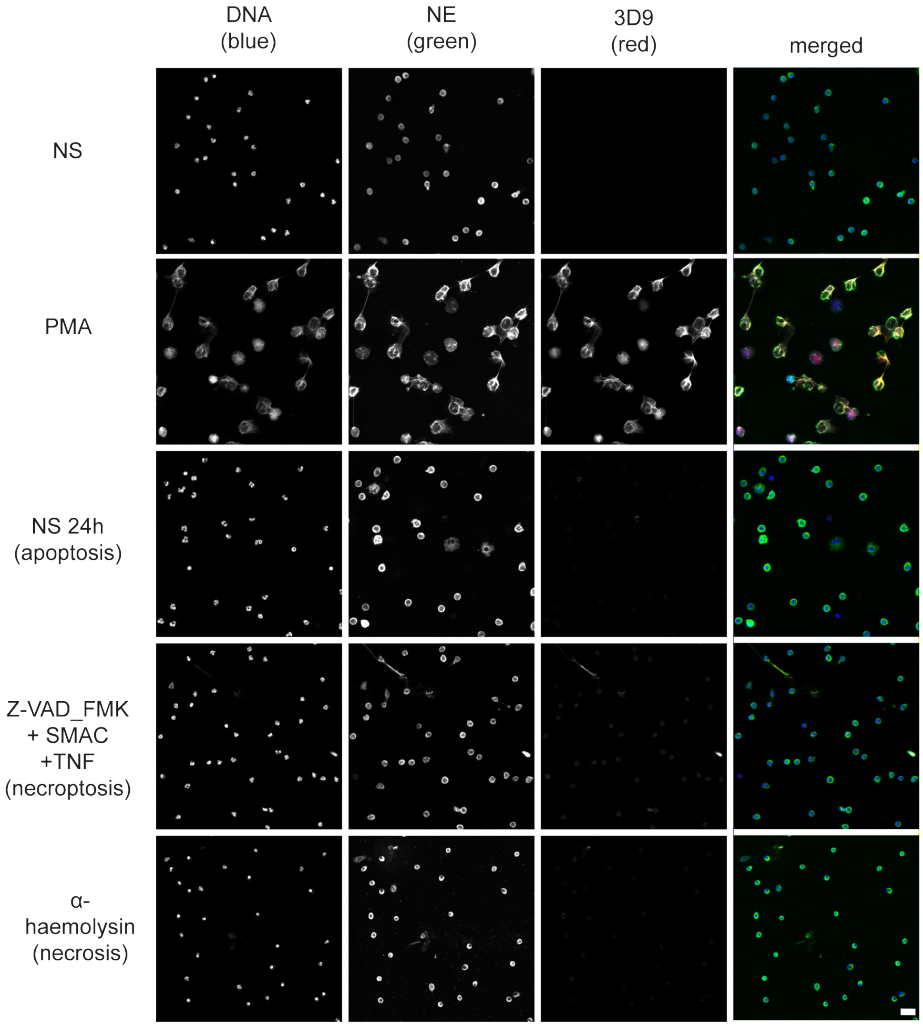

312

313 **Fig 7. Comparison of 3D9 detection in response to apoptotic, necroptotic & necrotic cell death stimuli.**
314 Confocal immunofluorescent microscopy of neutrophils stimulated with different cell death stimuli and
315 subsequently stained with Hoechst, anti-neutrophil elastase (NE) and 3D9. NETs were induced with PMA
316 (100 nM, 3h). Apoptosis was induced in resting neutrophils by incubation for 24h without stimulation
317 overnight. Neutrophils were stimulated with Z-VAD-FMK (50 μM) plus SMAC mimetic (100 nM) plus TNF (50
318 ng/ml) for 6h to induce necroptosis. Necrosis was induced with the pore forming toxin α-haemolysin (25
319 μg/ml). Images were taken at 20X and are representative of 3 experiments. Scalebar 20 μm. A comparison
320 was made with parallel samples stained with the chromatin antibody PL2.3 and are presented in S.Fig 7.

321 *3D9 labels NETs in human tissue sections*

322 NETs are found in inflamed tissues based on the juxtaposition of chromatin and granular makers

323 as well as the detection of citrullinated H3. 3D9 stains areas of decondensed DNA (Hoechst) that

324 colocalise with NE in both inflamed human tonsil (Fig. 8A) and human kidney (Fig. 8B). This

325 indicates that 3D9 labels NETs in histological samples - hematoxylin and eosin (HE) tissue
326 overviews are provided in the supplemental figures (S.Fig 8-10). Indeed, in kidney (Fig. 8C),
327 inflamed appendix (Fig. 9) and gallbladder (Fig. 10), 3D9 labelled DNA in the same cluster as anti-
328 H3cit or anti-H2B. Interestingly, 3D9 stained decondensed, more NET-like structures, while anti-
329 H3cit or anti-H2B antibodies stained relatively compact chromatin. Furthermore, colocalization
330 analysis of 3D9 with H2B or with H3cit revealed that 3D9 was more commonly colocalised with
331 H2B as compared to H3cit; overlap coefficients 0.463 (3D9-H2B) v 0.125 (3D9-H3cit), and 0.533
332 (3D9-H2B) v 0.122 (3D9-H3cit) for S.Fig 9 and 10 respectively.

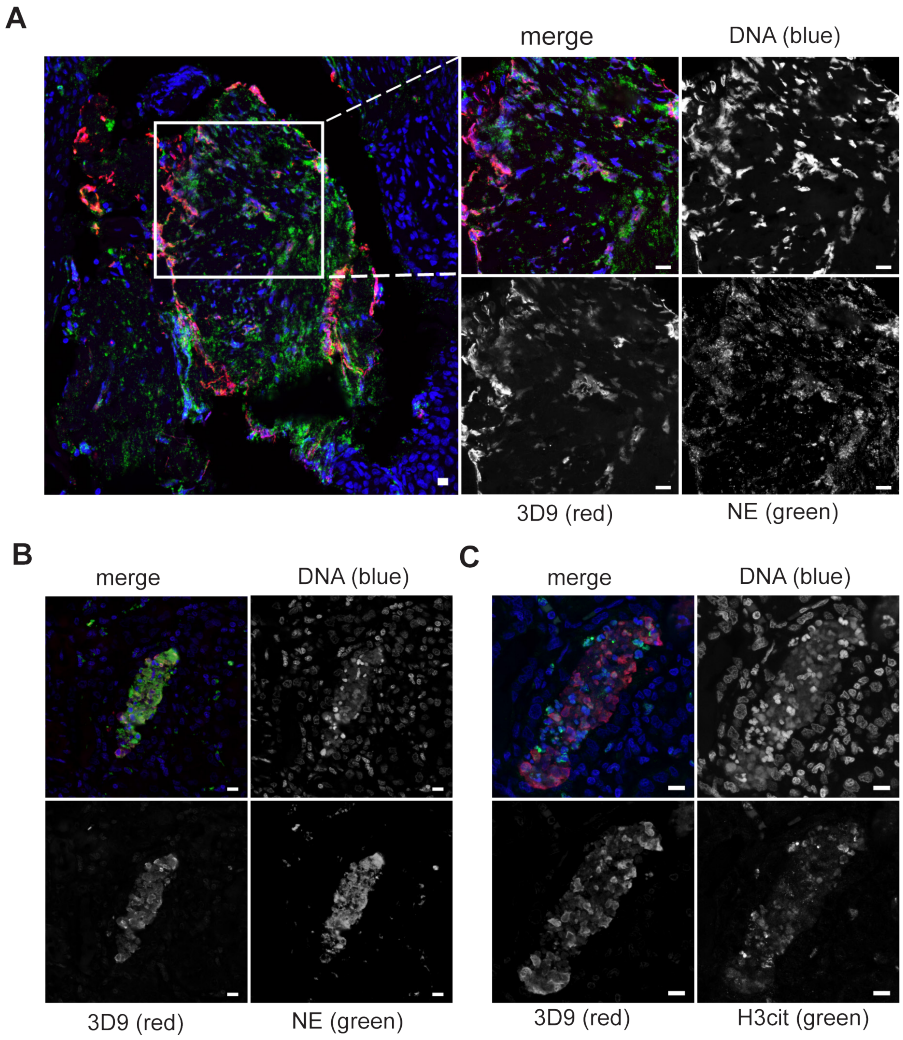

333

334 **Fig 8. Detection of clipped histone 3 & NETs in human tissues**
335 Paraffin embedded sections were stained with Hoechst, anti-NE and 3D9 or H3cit antibodies and examined
336 by confocal microscopy. Scale bar - 10 µm **(A)** inflamed human tonsil (**B** & **C**) Inflamed human kidney.

337

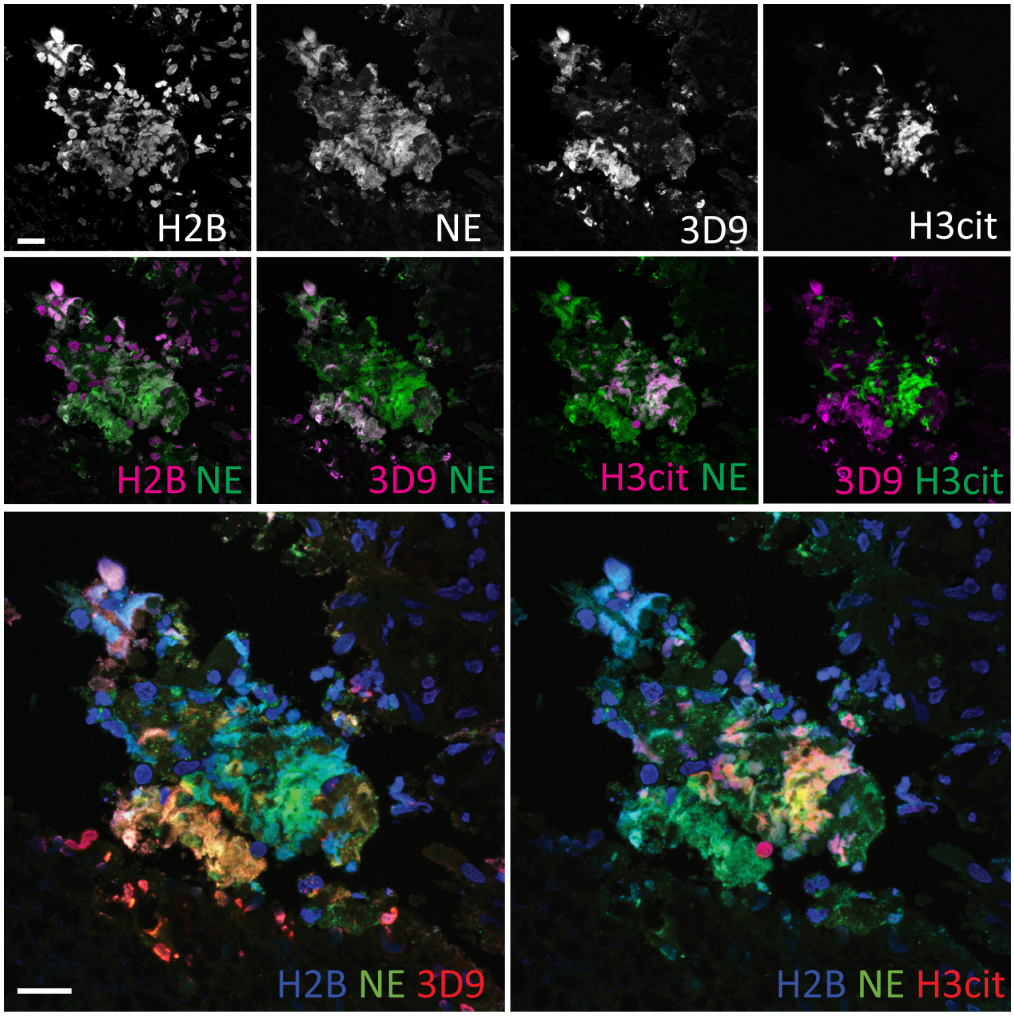

Fig. 9. Comparison of Clipped H3, H3cit & H2B staining in the gallbladder
Paraffin embedded sections were stained with Hoechst, anti-NE and histone antibodies 3D9, H3cit and H2B and examined by confocal microscopy. Scale bar – 20 µm.

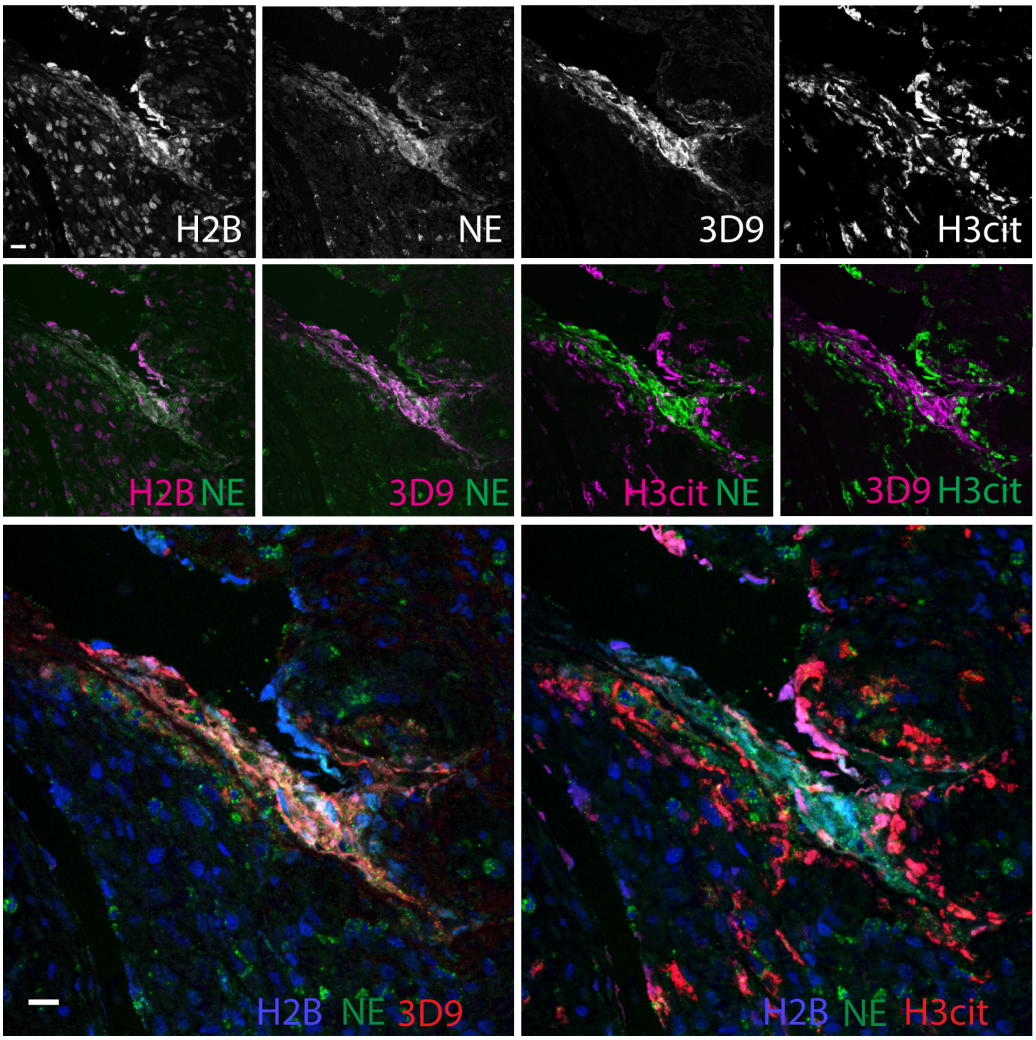

Fig. 10. Comparison of Clipped H3, H3cit & H2B staining in the appendix
Paraffin embedded sections were stained with Hoechst, anti-NE and 3D9 or H3cit antibodies and examined by confocal microscopy. Scale bar - 20 µm.

Discussion

Decondensed chromatin is a defining feature of NETs. It occurs through PTMs that partially neutralise the histone positive charge and thus the affinity of histones for negatively charged DNA (Papayannopoulos et al., 2010; Wang et al., 2009). One way to achieve this is through proteolytic removal of the lysine and arginine rich histone tails. Using a biochemical and proteomic approach, we determined that H3 is cleaved within its globular domain during NETosis. We exploited the

353 specificity of this event to produce a mouse monoclonal antibody to the *de novo* histone H3 epitope,
354 the new N-terminal beginning at R49. This antibody, 3D9, recognises human NETs induced by both
355 microbial and host derived physiological stimuli and distinguishes netotic neutrophils from
356 neutrophils that die via alternative pathways. It also discriminates between NETs and other cells in
357 mixed blood cell fractions and, importantly, NETs in human histological samples.

358 Until now, histone citrullination is the only PTM that has been used for antibody-based detection of
359 NETs. In this paper, we propose histone cleavage at H3R49 as a new histone PTM that can be
360 used for broad detection of NETs from human samples. The use of H3cit for the detection of NETs
361 is not without controversy. Not all NETs are citrullinated and NET formation can occur in the
362 absence or inhibition of citrullinating enzymes (Kenny et al., 2017; Konig and Andrade, 2016). By
363 identifying the precise histone cleavage site, we shed further light on this. The most commonly
364 used H3cit antibody detects citrullination of R2, R8 and R17. However, histone cleavage at R49
365 would remove the H3cit epitopes, rendering these NET defining PTMs mutually exclusive on a
366 single histone level. Indeed, co-staining by anti-H3cit and 3D9 in inflamed kidney, gallbladder and
367 appendix paraffin sections revealed extensive mutual exclusion of the two marks and more
368 abundant staining of decondensed chromatin by 3D9. Thus, we propose that 3D9 will allow broad
369 detection of NETs but may display a preference for more mature or proteolytically processed NETs.
370

371 In contrast to the present study, histone cleavage was reported as discriminating between different
372 pathways of NET formation (Pieterse et al., 2018). Using a sandwich ELISA approach, Pieterse *et*
373 *al* concluded that, generally, the N-terminal histone tails are removed in NOX dependent but not
374 NOX independent NET formation. They used a suite of N-terminal directed antibodies for H2B, H3
375 and H4, and all H3 epitopes were located N-terminal to the cleavage site H3R49. However, in the
376 final biological sample testing the authors did not examine H3. Interestingly, the authors observed
377 that, by immunofluorescent microscopy, all histone N-terminal antibodies failed to stain NETs at
378 time points after cell lysis. Therefore, to us, this data suggests that at later stages in NETosis the

379 histone N-terminal tails, at least for H3, are removed irrespective of the pathway of activation. This
380 is in line with our observations that both NOX dependent (PMA, heme) and NOX independent
381 (nigericin) stimuli result in NETs that are recognised by 3D9 and supports our finding that histone
382 H3 cleavage at R49 is a general feature of human NET formation.
383
384 In this study we detect NETs in fixed or denatured human samples from *in vitro* experiments and
385 histological samples. While an ELISA with 3D9 revealed a preference for NETs over isolated
386 chromatin or recombinant H3, immunoprecipitation of naïve cell lysates by 3D9 also pulled down
387 full length H3 as confirmed by immunoblot. It is not yet clear if this is due to co-immunoprecipitation
388 due to the presence of low levels of clipped histone or if this represents true recognition of intact
389 H3 by 3D9. Thus, care should be taken when detecting cleaved H3 or NETs under native and mild
390 detergent conditions and all sample types e.g. serum samples, need careful validation for cross
391 reactivity.
392
393 More broadly, and applying to the general principles of NET detection, it is not yet possible to prove
394 conclusively that the detected decondensed chromatin originates from the same cell source as the
395 neutrophil proteins which decorate it. For example, in an infected necrotic wound to which to high
396 numbers of neutrophils are recruited. Here, activated neutrophils might release both proteases
397 (Borregaard et al., 1993) and citrullinating enzymes (Spengler et al., 2015; Zhou et al., 2017) that
398 bind to and modify extracellular chromatin generating a NET - according to the histological
399 definition. This remains a conundrum that requires further exploration.
400
401 N-terminal histone cleavage at H3R49 is a novel and so far undescribed cleavage site in any
402 eukaryotic organism. Unusually, it is located in the globular rather than the unstructured tail region
403 of H3. H3R49 is one of 6 key residues important for the regulation of H3K36me^3 and forms part of
404 the structured nucleosome surface (Endo et al., 2012). Thus, we speculate that removal of the N-
405 terminal tail, in its entirety, could lead to removal of higher order structure interactions and facilitate

406 chromatin decondensation e.g. removal of H3K9me and its associated heterochromatin protein 1
407 interactions (Jacobs and Khorasanizadeh, 2002). To determine the contribution of histone cleavage
408 at H3R49 to the process of chromatin decondensation, future work will focus on establishing the
409 protease(s) responsible and the sequence of proteolytic events leading to this final truncation of
410 H3 and NET formation. Given the specificity of this event and its restriction to NETotic forms of cell
411 death, we propose that N-terminal cleavage at H3R49 is an example of histone 'clipping' in
412 neutrophils – a term proposed by the histone/histone proteolysis field for specific histone cleavage
413 sites for which a biological function has been demonstrated (Dhaenens et al., 2015).
414
415 In conclusion, this study represents the first identification of a distinctive and exclusive marker of
416 NETs and describes the development and characterisation of a complementary antibody to
417 facilitate easier detection of human NETs. Analogous to finding a smoking gun at a crime scene,
418 the monoclonal antibody 3D9 detects evidence of the proteolytic events that occur in NETosis –
419 the proteolytic signature, histone cleavage at H3R49. In doing so, 3D9 discriminates NETs from
420 chromatin of other cells and chromatin of neutrophils that die via alternative mechanisms. This
421 added layer of specificity will simplify the detection of NETs in tissue samples and facilitate
422 comparison of quantitative studies between labs. This will be an important step in assessing the
423 contribution of extracellular chromatin and NETs to disease pathology.
424

425 Materials and methods

426 *Reagents*

427 All reagents were purchased from common vendors of laboratory reagents e.g. Sigma Aldrich or
428 VWR Deutschland unless otherwise stated.

429 *Blood collection and ethical approval*

430 Venous blood was collected from healthy donors who had provided informed consent according to
431 the Declaration of Helsinki. Ethical approval was provided by the ethics committee of Charité-
432 Universitätsmedizin Berlin and blood was donated anonymously at Charité Hospital Berlin.

433 *Purification and culture of human peripheral blood neutrophils*

434 Neutrophils were isolated as described by Amulic et al (2017). Briefly, venous whole blood was
435 collected in EDTA and separated by layering over equal volume Histopaque 1119 and
436 centrifugation at 800 *g* (20 min). The pinkish neutrophil rich fraction was collected and washed once
437 by the addition of 3 volumes of wash buffer (PBS, without Mg^{2+} or Ca^{2+} [Gibco] supplemented with
438 0.5% [w/v] human serum albumin [HSA, Grifols]) and centrifugation at 300 *g* (10 min). The
439 neutrophil fraction was further purified by density gradient centrifugation - Percoll (Pharmacia)
440 gradient from 85%-65% (v/v). Purified cells were collected from the 80-70% fractions and washed
441 once before being resuspended in wash buffer. Cells were counted using a CASY cell counter.

442 For all experiments, unless indicated, neutrophils were cultured RPMI (GIBCO 32404014)
443 supplemented with 10 mM HEPES and 0.1% (w/v) HSA, which had been preequilibrated in CO_2
444 conditions for 1 h. For some stimuli, the HSA content was reduced to 0.05% or 0% HSA as indicated
445 in the figure legends. Cells were routinely cultured at 37°C, 5% CO_2 unless indicated. For all
446 experiments, stimuli were added to cell reactions as 10X working stock solutions freshly diluted in
447 RPMI. For inhibition experiments, a 10X inhibitor stock and appropriate vehicle controls, were
448 added to the cells and preincubated for the times stated in the figure legends.

449 *Neutrophil and NET lysate preparation*

450 To analyse proteins, lysates were prepared from stimulated or resting neutrophils. Cells were
451 seeded in culture medium in 1.5 ml microcentrifuge tubes at $1x10^7$ cells/ml with $5x10^6$ cells per time
452 point. After addition of the inhibitor or agonist, cells were gently mixed and incubated at 37 °C with
453 gentle rotation. At the specified time points, protease inhibitors - 1 mM AEBSF, 20 µM Cathepsin

454 G inhibitor I (Calbiochem), 20 μM neutrophil elastase inhibitor GW311616A (Biomol), 2X Halt
455 protease inhibitor cocktail (PIC, Thermofisher Scientific), 10 mM EDTA, 2 mM EGTA - were added
456 directly to the cell suspension. Cells were gently mixed and centrifuged at 1000 *g* (30 s) to collect
457 all residual liquid. Boiling 5X sample loading buffer (50 mM Tris-HCl pH 6.8, 2% [w/v] SDS, 10%
458 glycerol, 0.1% [w/v] bromophenol blue, 100 mM DTT) was added to samples which were then
459 briefly vortexed and boiled (98 °C) for 10 min and flash frozen in liquid nitrogen for storage at -
460 80 °C.

461 *1D SDS-PAGE and immunoblot blot*

462 For routine protein analysis, samples were analysed by 1D SDS-PAGE and immunoblotted.
463 Samples were thawed on ice, boiled at 98 °C (10 min) and sonicated to reduce viscosity (Braun
464 sonicator, 10 s, cycle 7, power 70%). Proteins were applied to NuPAGE 12% gels (Invitrogen,
465 Thermofisher) and run at 150 V in MES buffer (Thermofisher Scientific). Proteins were transferred
466 by western blot onto PVDF (0.2 μm pore size, Amersham GE Healthcare) using the BioRad wet
467 transfer system (buffer: 25 mM Tris, 192 mM glycine, 20% methanol, protocol: 30 min at 100 mA,
468 120 min at 400 mA). Blotting efficacy was assessed by Ponceau S staining. Blots were blocked
469 with TBST (TBS pH 7.5, 0.1% [v/v] Tween-20) with 5% [w/v] skimmed milk, for 1 h at RT. Blots
470 were then incubated with the following primary antibodies overnight at 4 °C or for 2 h at RT: rabbit
471 anti-histone H3 C-terminal pAb, 1:15000 (Active motif #61277); rat anti-histone H3 N-terminal mAb,
472 1:1000 (Active Motif #61647, aa 1-19); Histone H4 C-terminal, 1:5000 (Abcam 10158 – aa 50 to C
473 terminal); rabbit anti-histone H4 N-terminal mAb, 1:30,000 (Upstate, Millipore #05-858, aa17-28);
474 rabbit GAPDH mAb, 1:5000 (Cell Signalling Technology, #2118); mouse 3D9 1ug/ml (produced in
475 this study) – all diluted in TBST with 3% (w/v) skimmed milk. After washing with TBST (3 x 5 min),
476 blots were blocked for 15 min as before and then probed with secondary HRP conjugated
477 antibodies (Jackson ImmunoResearch -diluted 1:20000 in 5% skimmed milk TBST) for 1 h at RT.
478 Blots were washed in TBST (3 x 5 min) and developed using SuperSignal™ West Dura Extended
479 Duration Substrate (ThermoFisher Scientific) and an ImageQuant Gel imager (GE Healthcare).

480 *Immunofluorescent staining of in vitro samples*

481 For immunofluorescent imaging of purified cells, neutrophils/PBMCs were seeded in 24 well dishes
482 containing glass coverslips, with $1x10^5$ cells per well and incubated at 37 °C for 1 h to allow to
483 adhere to the coverslip. At this stage, inhibitors and priming factors were included as indicated.
484 Reactions were stopped by the addition of paraformaldehyde (2% [w/v]) for 20 min at RT or 4°C
485 overnight. After fixation, cells were washed and stained as previously described (Brinkmann et al
486 2012). Briefly, all steps were performed by floating inverted coverslips on drops of buffer on
487 laboratory parafilm. Cells were permeabilised with PBS, pH 7.5, 0.5% (v/v) Triton X-100 for 3 min.
488 For screening and quantification experiments, this permeabilization step was extended to 10 min.
489 Samples were washed (3 x 5 min) with PBS, 0.05% (v/v) Tween 20 and incubated with blocking
490 buffer - PBS pH 7.5, 0.05% (v/v) Tween 20, 3% (v/v) normal goat serum, 3% (w/v) freshwater fish
491 gelatin, 1% (w/v) BSA - for 20 min at RT and then probed with primary antibodies diluted in blocking
492 buffer and incubated overnight at 4 °C. Primary antibodies: anti-chromatin (H2A-H2B-DNA
493 complex) mouse mAb, 1 µg/ml (Losman 1992); neutrophil elastase, rabbit pAb 1:500 (Calbiochem);
494 mouse serum for screening, 1:100; hybridoma supernatants, neat; 3D9 mouse mAb, 1 µg/ml.
495 Samples were then washed as before. Alexa labelled secondary antibodies (Invitrogen) were
496 diluted 1/500 in blocking buffer and incubated for 2 h at RT. DNA was stained with Hoescht 33342
497 (Invitrogen, Molecular Probes) 1 ug/ml, incubated with the secondary antibody step. Samples were
498 washed in PBS followed by water and mounted in Mowiol mounting medium.

499 *Histone extraction from neutrophils*

500 Histone enriched fractions were prepared from resting neutrophils and NETs according to a method
501 modified from Shechter et al (2007). Neutrophils (4-8 $x10^7$) were resuspended in 13 ml of RPMI
502 (without HSA) in a 15 ml polypropylene tube and incubated on a roller at 37 °C with PMA 50 nM
503 for 90 min. After stimulation, 1 mM AEBSF was added to inhibit further degradation by NSPs and
504 cells were cooled on ice for 10 min. All subsequent steps were performed on ice or 4 °C where
505 possible. Cells and NETs were pelleted by centrifugation at 1000 *g*, 10 min. Samples were

506 resuspended in ice-cold hypotonic lysis buffer (10 mM Tris-HCl pH 8.0, 1 mM KCL, 1.5 mM $MgCl_2$,
507 1 mM DTT supplemented with protease inhibitors just before use – 1 mM AEBSF, 20 μM NEi, 20
508 μM CGi, 2X PIC, 10 mM EDTA) using 1 ml of buffer/$5x10^6$ cells. Cells were then incubated at 4 °C
509 on a rotator for 30 min before being passed through a syringe to aid lysis and shearing of intact
510 cells. Nuclei and NETs were collected by centrifugation at 10,000 *g*, 10 min, discarding the
511 supernatant. To disrupt nuclei, samples were resuspended in dH_2O (1 ml/$1x10^7$ cells)
512 supplemented with protease inhibitors, as before, and incubated on ice for 5 min with intermittent
513 vortexing. NP40 (0.2% [v/v]) was added to help lysis and disruption of NETs and samples were
514 sonicated briefly (10 s, mode 7, power 70%). To extract histones, H_2SO_4 (0.4 N) was added to
515 samples, and vortexed briefly. Samples were then incubated, rotating, for 2-3h. Histone enriched
516 fractions were collected by aliquoting samples into multiple 1.5 ml microcentrifuge tubes and
517 centrifuging at 16,000 *g* for 10 min, followed by collection of the supernatants. To minimise further
518 processing of histones, proteins were immediately precipitated overnight by dropwise addition of
519 trichloroacetic acid to a final concentration of 33% followed by mixing. The next day precipitated
520 proteins were pelleted by centrifugation at 16,000 *g*, 10 min. The supernatants were discarded and
521 waxy pellets were washed once with equal volume ice-cold acetone with 0.2% (v/v) HCl and 5
522 times with ice-cold acetone alone. Pellets were allowed to air dry for 5 min before being
523 resuspended with 1 ml (per $5x10^6$ cells) of dH_2O plus 1 mM AEBSF. For difficult to resuspend
524 pellets the mixture was vigorously shaken at 4°C overnight before samples were centrifuged, as
525 before, to remove undissolved protein. Pooled supernatants for each sample were lyophilised and
526 stored at -80°C until histone fractionation.

527 *Purification of histone H3*

528 Histones were fractionated by RP-HPLC according to the method described by Shechter et al
529 (2007). After lyophilisation samples were resuspended in 300 μl Buffer A (5% acetonitrile, 0.1%
530 trifluoroacetic acid) and centrifuged at 14,000 *g* to remove particulate matter. 150 μl of clarified
531 sample was mixed with 40 μl Buffer A before being applied to a C18 column (#218TP53, Grave

532 Vydac) and subjected to RP-HPLC (Waters 626 LC System, MA, US) as described by Schecter et
533 al (2007). The flow rate was set to 1 ml min^{-1} and fractions were collected at 30 s intervals from
534 minute 30 to 55. All fractions were lyophilised and stored at -80 °C until analysis. To determine
535 which fractions contained H3 and cleaved species, each fraction was dissolved in 50 µl dH_2O and
536 5 µl was subjected to SDS-PAGE and either stained with Coomassie blue stain or transferred to
537 PVDF and immunoblotted for H3 and H4 as described already.

538 *2D electrophoresis (2-DE) of purified histones*

539 To determine the cleavage sites, H3 containing fractions were pooled and subjected to a small gel
540 2-DE procedure (Jungblut and Seifert, 1990). Briefly, pooled fractions were denatured in 9 M urea,
541 70 mM DTT, 2% Servalyte 2-4 and 2 % Chaps. Samples (30 µl) were applied to 1.5 mm thick
542 isoelectric focusing (IEF) gels using ampholytes 7-9 and a shortened IEF protocol was used: 20
543 min 100 V, 20 min 200 V, 20 min 400 V, 15 min 600 V, 5 min 800 V, and 3 min 1000 V, (a total of
544 83 min and 500 Vh) in 8 cm long IEF tube gels. Separation in the second dimension was performed
545 in 6.5 cm x 8.5 cm x 1.5 mm SDS-PAGE gels. Duplicate gels were prepared; one stained with
546 Coomassie Brilliant Blue R250 for excision of spots for mass spectrometry identification; and the
547 second transferred to PVDF as follows. Proteins were blotted onto PVDF blotting membranes (0.2
548 µm) with a semidry blotting procedure (Jungblut et al., 1990) in a blotting buffer of 100 mM borate.
549 Spots were stained by Coomassie Brilliant Blue R250 and analysed by N-terminal Edman
550 degradation sequencing (Proteome Factory, Berlin, Germany).

551

552 *Antibody generation*

553 Immunising and screening peptides are outlined in S.Table 2 (S.Fig 3A) and were synthesized by
554 Eurogentec (Belgium). A portion was further conjugated to Key Lymphocyte Haemoglutinin (KLH)
555 for immunization. Immunisation of mice, preliminary ELISA screening and production of
556 hybridomas were performed by Genscript as follows. Six mice (3x Balb/c and 3x C57/BL6) were
557 immunized with branched peptides. Mice were bled and effective immunization was assessed using

558 a direct ELISA. The ELISA and subsequent inhouse immunoblot and immunofluorescent
559 microscopy screening strategy are outline in S.Fig 3A. Following selection of effectively immunized
560 animals, a further boost injection of the immunogen was given before isolation of spleen cells for
561 hybridoma production. The resulting hybridoma supernatants were screened similarly. Large-scale
562 culture of supernatants and purification of antibodies was performed by Genscript.

563 *ELISA*

564 To assess 3D9 specificity for NETs, 3D9 was used in an indirect ELISA to detect cleaved H3 in
565 purified NETs, chromatin, recombinant H3 and DNA. NETs were prepared by seeding $3x10^6$
566 neutrophils in a 6 well dish and incubating for 3-6 h with 100 nM PMA. NETs were gently washed
567 3 times with equal volume PBS, before being collected in 300 µl PBS. Clumped NETs were
568 disrupted by sonicating briefly (3 s, mode 7, power 70% - Braun Sonicator) and then snap frozen
569 and stored at -80°C. Chromatin was prepared from lung epithelial cells (A549) as previously
570 described by Shechter *et al* (2007). The final nuclear pellet was resuspended in dH_2O and
571 sonicated as before and stored at -80 °C. The DNA content of NETs and chromatin was assessed
572 by PicoGreen assay according to the manufacturer's instructions (Thermofisher Scientific).
573 Beginning at 1 µg/ml (of DNA content), serial dilutions of NETs, chromatin and calf thymus DNA
574 (Invitrogen) were prepared in lo-DNA bind Eppendorf microcentrifuge tubes. A similar dilution series
575 of recombinant histone H3 (New England Biolabs) was prepared starting at 1 µg/ml protein. All
576 dilutions were performed in PBS. One hundred microliters of each sample, in duplicate, at dilutions
577 1 ug/ml to 1 ng/ml, was aliquoted in a Nunc Maxisorb 96 well dish and immobilised overnight at
578 4°C, 250 rpm. The immunising peptide, REIRR (10ng/ml) was used as a positive control. The
579 following day all wells were washed 6 times with wash buffer (PBS, 0.05% Tween 20) and then
580 blocked with 200 µl of blocking solution (1% BSA in wash buffer) for 2 h (RT). Wells were washed
581 once with wash buffer and incubated with 100 µl of 3D9 (2 µg/ml, in blocking solution) at RT (2 h)
582 with gentle shaking (250 rpm). Wells were washed 6 times as before and then incubated with 100
583 µl of secondary HRP conjugated anti-mouse (Jackson laboratories) at 1:10,0000 dilution in blocking

584 solution and incubated as before. Finally, wells were washed 6 times as before and HRP activity
585 was detected using TMB (3,3', 5,5' tetramethylbenzidine) reagent (BD OptEIA™) according to the
586 manufacturer's instructions (incubating for 15 -30 min). The assay was stopped by the addition of
587 100 µl H_2SO_4 (0.16 M) and absorbance (450 nm) was measured on a 96 well plate reader
588 (VERSAmax, Molecular Devices, CA, US).

589 *Quantification of staining characteristics by Image J and R*

590 In order to assess staining characteristics of antibodies during NET formation we developed a
591 bundle of Image J and R scripts. These scripts allow for an automated workflow starting from 2-
592 channel microscopic images of an experimental series (DNA stain, antibody stain), to a graphical
593 representation and classification of individual cells and eventually to mapping these classifications
594 back to the original images as a graphical overlay. In the first step nuclei are segmented based on
595 intensity thresholding (either programmatic or manual), including options for lower and upper size
596 selection limits. The same threshold is applied to the entire experimental series and the upper size
597 limit is used to exclude fused structures that cannot be assigned individual cells. A quality score is
598 assigned to every image based on the fraction of the total DNA stained area that can be assigned
599 to individual cells (or NETs). This score along with all other parameters of the analysis is exported
600 as report file and can be used to automatically exclude images from the analysis. In addition, this
601 part of the script generates a result file that includes the area, circumference (as x,y coordinates)
602 and cumulative intensities for each channel for every detected nucleus along with information such
603 as time point or stimulus that can be assigned programmatically. In order to analyse these data
604 sets we implemented a series of functions in R. These functions include import of Image J result
605 files, classification of cells based on nuclear area and staining intensity, various plot and data export
606 functions, as well mapping functions that allow to display the classification of nuclei as color coded
607 circumferences overlaid on the original images. The scripts are available for download at
608 https://github.com/tulduro/NETalyser

609 *Quantification of NETs by Image J*

610 NETs were quantified by the semi-automatic method described by Brinkmann et al (2012) and via
611 a second modified method that allowed automatic quantification. All microscopy image datasets
612 were processed by both methods to allow comparison. Hoechst was used to stain total DNA and
613 NETs were additionally stained with anti-chromatin (PL2.3) or 3D9 antibodies (1 µg/ml) and Alexa-
614 568 coupled secondary antibody according to the previous section. Images were acquired with a
615 Leica DMR upright fluorescence microscope equipped with a Jenoptic B/W digital microscope
616 camera and 10x or 20x objective lens. For each experiment, the same exposure settings were used
617 for all samples and a minimum of 3 random fields of view (FOV) were collected. Images were
618 analysed using ImageJ/FIJI software. As described by Brinkmann et al (2012), each channel was
619 imported as an image sequence and converted into a stack. To count total cells/NETs per FOV,
620 the Hoechst channel stack was imported and segmented using the automatic thresholding function
621 (Bernsen method) with radius 15 and parameter 1 set to 35 to produce a black and white
622 thresholded image. Particle analysis was then performed to count all objects the size of a cell
623 nucleus or bigger (10x objective: particle size 25-infinity; 20x objective: particle size 100-infinity)
624 and to exclude background staining artefacts. Total NETs were then counted using the anti-
625 chromatin (PL2.3) or 3D9 channels accordingly. For the method published in 2012, anti-chromatin
626 stains were segmented using manually adjusted thresholding so that the less intense staining of
627 resting cell nuclei was excluded. Particle analysis was then performed to count all objects larger
628 than a resting cell nucleus (10x objective: particle size 75-infinity; 20x objective: particle size 250-
629 infinity). This was also performed for 3D9. In contrast, in the second analysis, the workflow was
630 modified so that the automatic Bernsen thresholding and segmentation were used for both Hoechst
631 and NET channels, total cells and NETs respectively. For each method percentage NETs were
632 calculated as (NETs/Total cells) x100. Results per FOV were then averaged according to sample.
633 A schematic of the different workflows is presented in S.Fig 5.

634 *Immunofluorescent staining of histological samples from tissue sections*

635 Paraffin sections (2 µm thick) were deparaffinized in two changes of 100% xylene for 5 min each
636 and then rehydrated in two changes of 100% ethanol for 5 min each and followed by 90% and 70%
637 ethanol for 5 min each. Sections were washed with 3 changes of deionized water and incubation
638 in TBS (Tris buffered saline). For antigen retrieval, Target Retrieval Solution (TRS pH9) (Dako
639 S2367) was used to incubate the slides in a steam cooker (Braun) for 20 min. After cooling down
640 to room temperature in antigen retrieval buffer, slides were rinsed 3x in deionized water and
641 incubated in TBS until further processing. Slides were blocked with blocking buffer (1% BSA, 5%
642 normal donkey serum, 5% cold water fish gelatin and 0.05% Tween20 in TBS, pH7.4) for 30 min.
643 Blocking buffer was removed, and sections were incubated with primary antibodies at appropriate
644 dilution in blocking buffer (containing 0.05% Triton-X100) overnight at RT. Sections were rinsed in
645 TBS and then incubated with secondary antibody at an appropriate concentration (1:100) for 45
646 min in the dark at RT and then rinsed three times in TBS for 5 min followed by rinsing with deionized
647 water. Slides were incubated with DNA stain Hoechst 33342 (1:5000) for 5 min, rinsed with water
648 before mounting with Mowiol. Primary antibodies for detection of NETs were as follows: mouse
649 anti-cleaved histone 3 clone 3D9 (2 µg/ml); rabbit anti-histone H3 antibody (citrulline R2 + R8 +
650 R17; ab5103, Abcam); chicken anti-Histone H2B ab134211 Abcam (1:400); sheep anti-ELANE
651 (NE) LS-Bio LSB 4244 Lot 75251. Secondary antibodies were the following: donkey anti-rabbit
652 immunoglobulin G (IgG) heavy and light chain (H&L) Alexa Fluor 488 (Jackson 711-225-152); and
653 donkey anti-mouse IgG H&L Cy3 (Jackson 715-165-151); donkey anti-sheep (IgG) H&L Alexa Fluor
654 647 (Jackson 713-605-147). An upright widefield microscope (Leica DMR) equipped with a
655 JENOPTIK B/W digital microscope camera or a Leica confocal microscope SP8 were used for
656 fluorescent imaging. Z-stack images were collected at 63× magnification. Where stated
657 colocalisation analysis was performed on confocal images using Volocity 6.5.1 software. Human
658 tonsil and kidney paraffin tissue blocks were purchased from AMSbio. Inflamed tissue from a
659 gallbladder and an appendix was obtained from archived leftover paraffin embedded diagnostic

660 samples and used in an anonymised way after approval through the Charité Ethics Committee
661 (Project EA4/124/19, July 24, 2019). Informed consent from patients for use of biomaterials for
662 research was obtained as part of the institutional treatment contract at Charité.

663 *Contributions*

664 DOT- Conceptualization, methodology, investigation, data curation, figure preparation, writing
665 original draft, review and editing; UZA - 2-DE, blotting and sample preparation for protein
666 sequencing; UA -preparation of human pathology tissue samples and microscopy of tissue
667 samples, image curation; MS - MALDI mass spectrometry; SF - provision and description of human
668 pathology tissues and advice on histology figure presentation; PRJ - proteomic and 2-DE analysis;
669 VB - colocalisation analysis, image curation, reviewing and critical feedback on manuscript; AH -
670 conceptualization, data curation for R analysis, R scripting; AZ- conceptualization, reviewing and
671 editing of manuscript; AZ and AH provided critical feedback to DOT and helped shape the research,
672 analysis and manuscript.

673 *Acknowledgements*

674 The authors would like to give special thanks to Borko Amulic and Gerben Marsman for their critical
675 feedback at the early stages of manuscript preparation.

676 *Competing interests*

677 DOT, AH and AZ and the Max Planck Society have submitted a patent application concerning the
678 contents of this manuscript.

679 *List of supplemental figures*

680 **S.Fig 1A.** Cysteine protease inhibition by E64 does not inhibit histone H3 cleavage.
681 **S.Fig 1B.** AEBSF does not inhibit ROS production & is not cytotoxic.
682 **S.Fig 2A.** Schematic summary of extraction & identification of histone H3 cleavage sites in NETs.
683 **S.Fig 2B.** Separation of histone H3 by two dimensional electrophoresis & protein identification by
684 mass spectrometry (contains **S.Table 1**)

685 **S.Fig 3A.** Outline of immunisation & screening strategy for antibody production (contains **S.Table**
686 **2**)
687 **S.Fig 3B.** Peptide inhibition of 3D9 binding to NETs
688 **S.Fig 3C.** 3D9 immunoprecipitation
689 **S.Fig 4A.** Binding profiles recorded for 3D9 on the linear peptide array.
690 **S.Fig 4B.** Binding profiles recorded for 3D9 on helical peptide mimics arrays
691 **S.Table 3.** Summary of identified 3D9 binding regions in the peptide array.
692 **S.Fig 4C**. Fine epitope mapping by replacement analysis & visualisation of the 3D9 epitope in the
693 nucleosome core complex.
694 **S.Fig 5.** Workflow of NET analysis methods
695 **S.Fig 7.** Comparison of PL2.3 detection in response to apoptotic, necroptotic & necrotic cell death
696 stimuli
697 **S.Fig 8.** Hematoxylin & eosin (HE) stain of kidney section
698 **S.Fig 9.** Hematoxylin & eosin (HE) stain of gallbladder & colocalization analysis
699 **S.Fig 10.** Hematoxylin & eosin stain of inflamed appendix & colocalization analysis.
700

701 *Supplemental files*

702 S.file 1. Peptides for epitope mapping
703 S.file 2. Supplemental Methods
704 S.file 3. Supplemental Results
705

706 *References*

707 Albrengues, J., Shields, M.A., Ng, D., Park, C.G., Ambrico, A., Poindexter, M.E., Upadhyay, P.,
708 Uyeminami, D.L., Pommier, A., Kuttner, V.*, et al.* (2018). Neutrophil extracellular traps produced
709 during inflammation awaken dormant cancer cells in mice. Science *361*.
710 10.1126/science.aao4227

711 Amulic, B., Knackstedt, S.L., Abu Abed, U., Deigendesch, N., Harbort, C.J., Caffrey, B.E.,
712 Brinkmann, V., Heppner, F.L., Hinds, P.W., and Zychlinsky, A. (2017). Cell-Cycle Proteins Control
713 Production of Neutrophil Extracellular Traps. Dev Cell *43*, 449-462 e445.
714 10.1016/j.devcel.2017.10.013

715 Bannister, A.J., and Kouzarides, T. (2011). Regulation of chromatin by histone modifications. Cell
716 Res *21*, 381-395. 10.1038/cr.2011.22

717 Bianchi, M., Hakkim, A., Brinkmann, V., Siler, U., Seger, R.A., Zychlinsky, A., and Reichenbach,
718 J. (2009). Restoration of NET formation by gene therapy in CGD controls aspergillosis. Blood
719 *114*, 2619-2622. 10.1182/blood-2009-05-221606.

720 Borregaard, N., Lollike, K., Kjeldsen, L., Sengelov, H., Bastholm, L., Nielsen, M.H., and Bainton,
721 D.F. (1993). Human neutrophil granules and secretory vesicles. Eur J Haematol *51*, 187-198.
722 10.1111/j.1600-0609.1993.tb00629.x.

723 Brinkmann, V., Goosmann, C., Kuhn, L.I., and Zychlinsky, A. (2012). Automatic quantification of
724 in vitro NET formation. Frontiers in immunology *3*, 413. 10.3389/fimmu.2012.00413.

725 Brinkmann, V., Reichard, U., Goosmann, C., Fauler, B., Uhlemann, Y., Weiss, D.S., Weinrauch,
726 Y., and Zychlinsky, A. (2004). Neutrophil extracellular traps kill bacteria. Science *303*, 1532-1535.
727 10.1126/science.1092385

728 Chakravarthy, S., Luger, K. (2005). Nucleosomes containing the histone domain of macroH2A: In
729 vitro possibilities. 10.2210/pdb2f8n/pdb

730 Cools-Lartigue, J., Spicer, J., McDonald, B., Gowing, S., Chow, S., Giannias, B., Bourdeau, F.,
731 Kubes, P., and Ferri, L. (2013). Neutrophil extracellular traps sequester circulating tumor cells
732 and promote metastasis. The Journal of clinical investigation. 10.1172/JCI67484

733 Dabrowska, D., Jablonska, E., Iwaniuk, A., and Garley, M. (2019). Many Ways-One Destination:
734 Different Types of Neutrophils Death. Int Rev Immunol *38*, 18-32.
735 10.1080/08830185.2018.1540616

736 Demers, M., Wong, S.L., Martinod, K., Gallant, M., Cabral, J.E., Wang, Y., and Wagner, D.D.
737 (2016). Priming of neutrophils toward NETosis promotes tumor growth. Oncoimmunology *5*,
738 e1134073. 10.1080/2162402X.2015.1134073

739 Dhaenens, M., Glibert, P., Meert, P., Vossaert, L., and Deforce, D. (2015). Histone proteolysis: a
740 proposal for categorization into 'clipping' and 'degradation'. Bioessays *37*, 70-79.
741 10.1002/bies.201400118

742 Diatchuk, V., Lotan, O., Koshkin, V., Wikstroem, P., and Pick, E. (1997). Inhibition of NADPH
743 oxidase activation by 4-(2-aminoethyl)-benzenesulfonyl fluoride and related compounds. The
744 Journal of biological chemistry *272*, 13292-13301. 10.1074/jbc.272.20.13292.

745 Duncan, E.M., Muratore-Schroeder, T.L., Cook, R.G., Garcia, B.A., Shabanowitz, J., Hunt, D.F.,
746 and Allis, C.D. (2008). Cathepsin L proteolytically processes histone H3 during mouse embryonic
747 stem cell differentiation. Cell *135*, 284-294. 10.1016/j.cell.2008.09.055

748 Endo, H., Nakabayashi, Y., Kawashima, S., Enomoto, T., Seki, M., and Horikoshi, M. (2012).
749 Nucleosome surface containing nucleosomal DNA entry/exit site regulates H3-K36me3 via
750 association with RNA polymerase II and Set2. Genes Cells *17*, 65-81. 10.1111/j.1365-
751 2443.2011.01573.x

752 Galluzzi, L., Vitale, I., Abrams, J.M., Alnemri, E.S., Baehrecke, E.H., Blagosklonny, M.V.,
753 Dawson, T.M., Dawson, V.L., El-Deiry, W.S., Fulda, S.*, et al.* (2012). Molecular definitions of cell
754 death subroutines: recommendations of the Nomenclature Committee on Cell Death 2012. Cell
755 Death Differ *19*, 107-120. 10.1038/cdd.2011.96

756 Gavillet, M., Martinod, K., Renella, R., Harris, C., Shapiro, N.I., Wagner, D.D., and Williams, D.A.
757 (2015). Flow cytometric assay for direct quantification of neutrophil extracellular traps in blood
758 samples. Am J Hematol *90*, 1155-1158. 10.1002/ajh.24185

759 Hacbarth, E., and Kajdacsy-Balla, A. (1986). Low density neutrophils in patients with systemic
760 lupus erythematosus, rheumatoid arthritis, and acute rheumatic fever. Arthritis and rheumatism
761 *29*, 1334-1342. 10.1002/art.1780291105.

762 Hakkim, A., Fuchs, T.A., Martinez, N.E., Hess, S., Prinz, H., Zychlinsky, A., and Waldmann, H.
763 (2011). Activation of the Raf-MEK-ERK pathway is required for neutrophil extracellular trap
764 formation. Nat Chem Biol *7*, 75-77. 10.1038/nchembio.496.

765 Howe, C.G., and Gamble, M.V. (2015). Enzymatic cleavage of histone H3: a new consideration
766 when measuring histone modifications in human samples. Clin Epigenetics *7*, 7. 10.1186/s13148-
767 014-0041-5

768 Jacobs, S.A., and Khorasanizadeh, S. (2002). Structure of HP1 chromodomain bound to a lysine
769 9-methylated histone H3 tail. Science *295*, 2080-2083. 10.1126/science.1069473

770 Jimenez-Alcazar, M., Kim, N., and Fuchs, T.A. (2017). Circulating Extracellular DNA: Cause or
771 Consequence of Thrombosis? Seminars in thrombosis and hemostasis. 10.1055/s-0036-1597284

772 Jungblut, P., Eckerskorn, C., Lottspeich, F., and Klose, J. (1990). Blotting efficiency investigated
773 by using two-dimensional electrophoresis, hydrophobic membranes and proteins from different
774 sources. Electrophoresis *11*, 581-588. 10.1002/elps.1150110709

775 Jungblut, P.R., and Seifert, R. (1990). Analysis by high-resolution two-dimensional
776 electrophoresis of differentiation-dependent alterations in cytosolic protein pattern of HL-60
777 leukemic cells. J Biochem Biophys Methods *21*, 47-58. 10.1016/0165-022x(90)90044-d.

778 Kenny, E.F., Herzig, A., Kruger, R., Muth, A., Mondal, S., Thompson, P.R., Brinkmann, V.,
779 Bernuth, H.V., and Zychlinsky, A. (2017). Diverse stimuli engage different neutrophil extracellular
780 trap pathways. Elife *6*. 10.7554/eLife.24437.

781 Knackstedt, S.L., Georgiadou, A., Apel, F., Abu-Abed, U., Moxon, C.A., Cunnington, A.J.,
782 Raupach, B., Cunningham, D., Langhorne, J., Kruger, R.*, et al.* (2019). Neutrophil extracellular
783 traps drive inflammatory pathogenesis in malaria. Science immunology *4*.
784 10.1126/sciimmunol.aaw0336

785 Kobayashi, S.D., Voyich, J.M., Whitney, A.R., and DeLeo, F.R. (2005). Spontaneous neutrophil
786 apoptosis and regulation of cell survival by granulocyte macrophage-colony stimulating factor.
787 Journal of leukocyte biology *78*, 1408-1418. 10.1189/jlb.0605289

788 Konig, M.F., and Andrade, F. (2016). A Critical Reappraisal of Neutrophil Extracellular Traps and
789 NETosis Mimics Based on Differential Requirements for Protein Citrullination. Frontiers in
790 immunology *7*, 461. 10.3389/fimmu.2016.00461

791 Losman, M.J., Fasy, T.M., Novick, K.E., and Monestier, M. (1992). Monoclonal autoantibodies to
792 subnucleosomes from a MRL/Mp(-)+/+ mouse. Oligoclonality of the antibody response and
793 recognition of a determinant composed of histones H2A, H2B, and DNA. Journal of immunology
794 (Baltimore, Md : 1950) *148*, 1561-1569. (*DOI not assigned*)

795 Melo, F.R., Vita, F., Berent-Maoz, B., Levi-Schaffer, F., Zabucchi, G., and Pejler, G. (2014).
796 Proteolytic histone modification by mast cell tryptase, a serglycin proteoglycan-dependent
797 secretory granule protease. The Journal of biological chemistry *289*, 7682-7690.
798 10.1074/jbc.M113.546895

799 Neeli, I., and Radic, M. (2013). Opposition between PKC isoforms regulates histone deimination
800 and neutrophil extracellular chromatin release. Frontiers in immunology *4*, 38.
801 10.3389/fimmu.2013.00038

802 Papayannopoulos, V. (2018). Neutrophil extracellular traps in immunity and disease. Nat Rev
803 Immunol *18*, 134-147. 10.1038/nri.2017.105

804 Papayannopoulos, V., Metzler, K.D., Hakkim, A., and Zychlinsky, A. (2010). Neutrophil elastase
805 and myeloperoxidase regulate the formation of neutrophil extracellular traps. J Cell Biol *191*, 677-
806 691. 10.1083/jcb.201006052

807 Pertiwi, K.R., de Boer, O.J., Mackaaij, C., Pabittei, D.R., de Winter, R.J., Li, X., and van der Wal,
808 A.C. (2018). Extracellular traps derived from macrophages, mast cells, eosinophils and

809 neutrophils are generated in a time-dependent manner during atherothrombosis. The Journal of
810 pathology. 10.1002/path.5212

811 Pieterse, E., Rother, N., Yanginlar, C., Gerretsen, J., Boeltz, S., Munoz, L.E., Herrmann, M.,
812 Pickkers, P., Hilbrands, L.B., and van der Vlag, J. (2018). Cleaved N-terminal histone tails
813 distinguish between NADPH oxidase (NOX)-dependent and NOX-independent pathways of
814 neutrophil extracellular trap formation. Annals of the rheumatic diseases *77*, 1790-1798.
815 10.1136/annrheumdis-2018-213223

816 Posthumus, W.P., Lenstra, J.A., Schaaper, W.M., van Nieuwstadt, A.P., Enjuanes, L., and
817 Meloen, R.H. (1990). Analysis and simulation of a neutralizing epitope of transmissible
818 gastroenteritis virus. J Virol *64*, 3304-3309. 10.1128/JVI.64.7.3304-3309.1990.

819 Saitoh, T., Komano, J., Saitoh, Y., Misawa, T., Takahama, M., Kozaki, T., Uehata, T., Iwasaki, H.,
820 Omori, H., Yamaoka, S.*, et al.* (2012). Neutrophil extracellular traps mediate a host defense
821 response to human immunodeficiency virus-1. Cell Host Microbe *12*, 109-116.
822 10.1016/j.chom.2012.05.015

823 Schauer, C., Janko, C., Munoz, L.E., Zhao, Y., Kienhofer, D., Frey, B., Lell, M., Manger, B., Rech,
824 J., Naschberger, E.*, et al.* (2014). Aggregated neutrophil extracellular traps limit inflammation by
825 degrading cytokines and chemokines. Nature medicine *20*, 511-517. 10.1038/nm.3547

826 Schonrich, G., Kruger, D.H., and Raftery, M.J. (2015). Hantavirus-induced disruption of the
827 endothelial barrier: neutrophils are on the payroll. Frontiers in microbiology *6*, 222.
828 10.3389/fmicb.2015.00222

829 Shechter, D., Dormann, H.L., Allis, C.D., and Hake, S.B. (2007). Extraction, purification and
830 analysis of histones. Nat Protoc *2*, 1445-1457. 10.1038/nprot.2007.202

831 Sollberger, G., Tilley, D.O., and Zychlinsky, A. (2018). Neutrophil Extracellular Traps: The Biology
832 of Chromatin Externalization. Dev Cell *44*, 542-553. 10.1016/j.devcel.2018.01.019

833 Spengler, J., Lugonja, B., Ytterberg, A.J., Zubarev, R.A., Creese, A.J., Pearson, M.J., Grant,
834 M.M., Milward, M., Lundberg, K., Buckley, C.D.*, et al.* (2015). Release of Active Peptidyl Arginine
835 Deiminases by Neutrophils Can Explain Production of Extracellular Citrullinated Autoantigens in
836 Rheumatoid Arthritis Synovial Fluid. Arthritis & rheumatology (Hoboken, NJ) *67*, 3135-3145. doi:
837 10.1002/art.39313

838 Urban, C.F., Ermert, D., Schmid, M., Abu-Abed, U., Goosmann, C., Nacken, W., Brinkmann, V.,
839 Jungblut, P.R., and Zychlinsky, A. (2009). Neutrophil extracellular traps contain calprotectin, a

840 cytosolic protein complex involved in host defense against Candida albicans. PLoS Pathog *5*,
841 e1000639. 10.1371/journal.ppat.1000639

842 Urban, C.F., Reichard, U., Brinkmann, V., and Zychlinsky, A. (2006). Neutrophil extracellular
843 traps capture and kill Candida albicans yeast and hyphal forms. Cell Microbiol *8*, 668-676.

844 Wang, Y., Li, M., Stadler, S., Correll, S., Li, P., Wang, D., Hayama, R., Leonelli, L., Han, H.,
845 Grigoryev, S.A.*, et al.* (2009). Histone hypercitrullination mediates chromatin decondensation and
846 neutrophil extracellular trap formation. J Cell Biol *184*, 205-213. 10.1083/jcb.200806072

847 Yoo, D.G., Winn, M., Pang, L., Moskowitz, S.M., Malech, H.L., Leto, T.L., and Rada, B. (2014).
848 Release of cystic fibrosis airway inflammatory markers from Pseudomonas aeruginosa-stimulated
849 human neutrophils involves NADPH oxidase-dependent extracellular DNA trap formation. Journal
850 of immunology (Baltimore, Md : 1950) *192*, 4728-4738. 10.4049/jimmunol.1301589

851 Yoshida, M., Sasaki, M., Sugisaki, K., Yamaguchi, Y., and Yamada, M. (2013). Neutrophil
852 extracellular trap components in fibrinoid necrosis of the kidney with myeloperoxidase-ANCA-
853 associated vasculitis. Clin Kidney J *6*, 308-312. 10.1093/ckj/sft048

854 Zenaro, E., Pietronigro, E., Della Bianca, V., Piacentino, G., Marongiu, L., Budui, S., Turano, E.,
855 Rossi, B., Angiari, S., Dusi, S.*, et al.* (2015). Neutrophils promote Alzheimer's disease-like
856 pathology and cognitive decline via LFA-1 integrin. Nature medicine *21*, 880-886.
857 10.1038/nm.3913

858 Zhou, Y., Chen, B., Mittereder, N., Chaerkady, R., Strain, M., An, L.L., Rahman, S., Ma, W., Low,
859 C.P., Chan, D.*, et al.* (2017). Spontaneous Secretion of the Citrullination Enzyme PAD2 and Cell
860 Surface Exposure of PAD4 by Neutrophils. Frontiers in immunology *8*, 1200.
861 10.3389/fimmu.2017.01200